ADVANCED ENERGY MATERIALS
www.advenergymat.de

Deciphering the Role of Nickel in Electrochemical Organic Oxidation Reactions

Suptish Ghosh, Debabrata Bagchi, Indranil Mondal, Tobias Sontheimer, Rajenahally V. Jagadeesh, and Prashanth. W. Menezes**

Organic oxidation reactions (OORs) powered by renewable energy sources are gaining importance as a favorable alternative to oxygen evolution reaction, with the promise of reducing the cell potential and enhancing the overall viability of the water electrolysis. This comprehensive review delves into the electrochemical oxidation of diverse organic compounds, including alcohols, aldehydes, amines, and urea, as well as biomass-derived renewable feedstocks such as hydroxymethylfurfural and glycerol. The key focus centers on the role of nickel (Ni)-based catalysts for these OORs. The unique redox activity and chemical nature of Ni have been proven instrumental for the sustainable and cost-effective oxidation of various organic molecules more efficiently and selectively. This review article discusses how strategic choices, such as the selection of foreign metals, intercalating species, vacancies, defects, and a secondary element (e.g. chalcogens and non-metals), contribute to tuning the electrochemical performances of a Ni-based (pre)catalyst for OORs. Moreover, this review provides insights into the active species in various reaction environments and further explores reaction mechanisms, to apparent phase changes of the catalyst with the most relevant examples. Finally, the review not only elucidates the limitations of the current approaches but also outlines potential avenues for future advancements in OOR.

1. Introduction

The scarcity of carbon-positive fuel sources and the associated health hazards resulting from numerous chemical transformations urge the development of sustainable and low-cost methods capable of minimizing energy consumption, as well as waste generation.[1,2] An alternative to conventional fossil fuel is molecular hydrogen (H_2), which is a high-density energy carrier that reacts to oxygen (O_2) and releases an enormous amount of energy.[3] Notably, the electricity generated through this process produces only water as a by-product, rendering it a green and cleaner technique. In this regard, electrochemical water splitting, particularly in alkaline conditions, stands out as an efficient and environmentally benign approach for green hydrogen production. However, a critical bottleneck of this process lies in the sluggish kinetics of the anodic

S. Ghosh, P. W. Menezes
Department of Chemistry, Metalorganics and Inorganic Materials
Technische Universität Berlin
Straße des 17 Juni 115, Sekr. C2, 10623 Berlin, Germany
E-mail: prashanth.menezes@mailbox.tu-berlin.de

D. Bagchi, P. W. Menezes
Materials Chemistry Group for Thin Film Catalysis – CatLab
Helmholtz-Zentrum Berlin für Materialien und Energie
Albert-Einstein-Str. 15, 12489 Berlin, Germany

I. Mondal
School of Chemistry
Indian Institute of Science Education and Research Thiruvananthapuram
Thiruvananthapuram, Kerala 695551, India

The ORCID identification number(s) for the author(s) of this article can be found under https://doi.org/10.1002/aenm.202400696

DOI: 10.1002/aenm.202400696

T. Sontheimer
Strategy Department of Energy and Information
Helmholtz-Zentrum Berlin für Materialien und Energie
Hahn-Meitner-Platz 1, 14109 Berlin, Germany

R. V. Jagadeesh
Catalysis for Sustainable Syntheses
Leibniz-Institut für Katalyse e.V.
Albert-Einstein-Straße 29A, 18059 Rostock, Germany
E-mail: jagadeesh.rajenahally@catalysis.de

R. V. Jagadeesh
Nanotechnology Centre
Centre of Energy and Environmental Technologies
VŠB-Technical University of Ostrava
17. Listopadu 2172/15, Ostrava-Poruba 70800, Czech Republic

R. V. Jagadeesh
Department of Chemistry
REVA University
Bangalore 560064, India

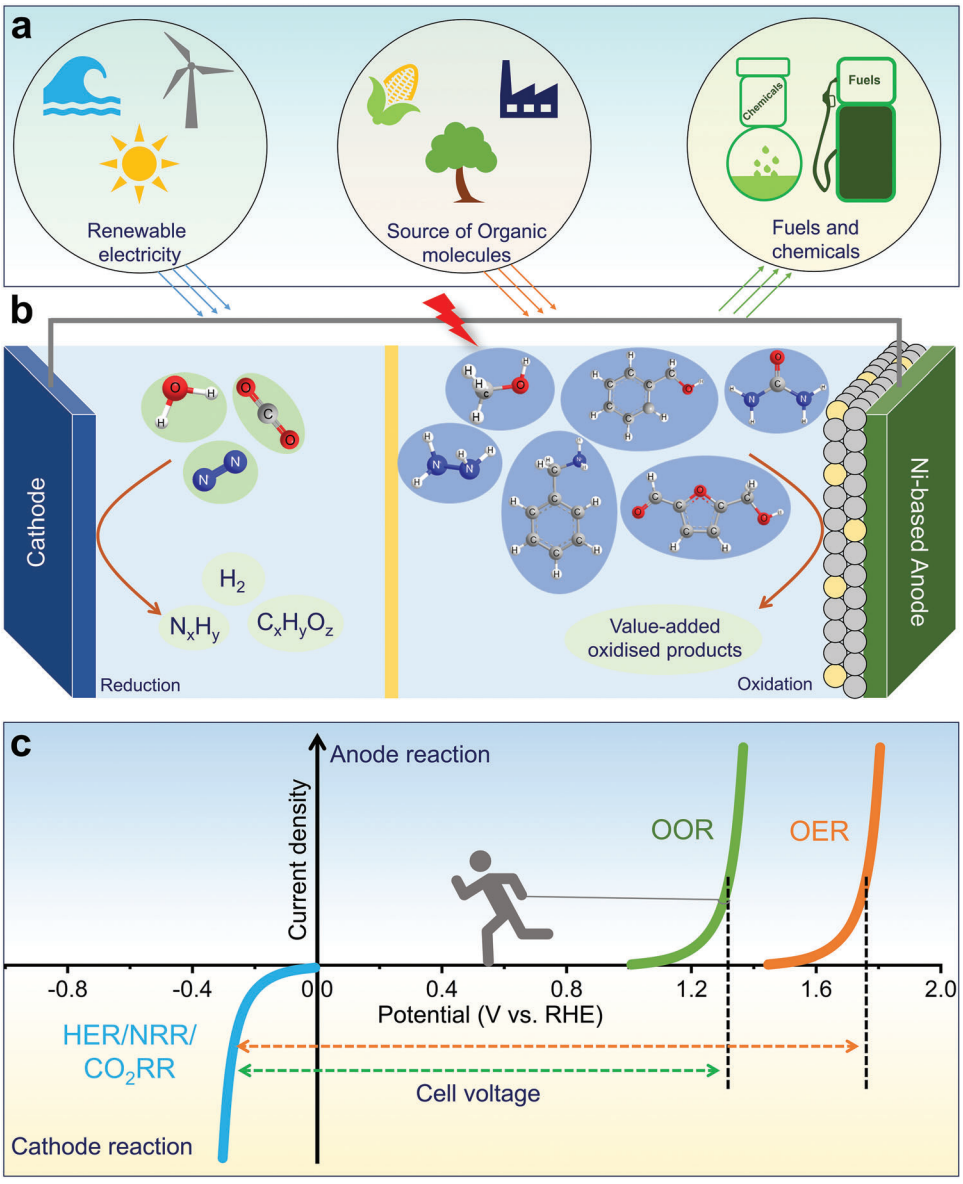

Figure 1. a) Electrochemical valorization of organic molecules derived from biomass and other feedstocks using renewable electricity. b) Schematic representation of the Ni-based electrode coupled with the valuable HER, CO_2RR, and NRR. c) Schematic comparison of potential ranges of OER and organic oxidation reaction (OOR) with the valuable cathodic reactions.

reaction, oxygen evolution reaction (OER), which leads to insufficient proton (H^+) and electron transfer into the cathode.[4–9] While various anode materials, particularly Fe-containing bimetallic catalysts, have demonstrated excellent OER activity,[6,10,11] their practical utility is hindered by their stability and complex dynamic nature, leading to a loss of activity over prolonged industrially relevant operation conditions.[12–14] To address this challenge, there has been a growing interest in replacing OER with the oxidation of protic organic compounds as an attractive pathway to supply H^+ and electrons without requiring large operating potentials (see **Figure 1**).[15–18] This approach received more technological importance as a wide variety of cathode reactions, like electrochemical CO_2 reduction (CO_2RR) or nitrogen reduction reaction (NRR), resulting in the synthesis of valuable fine and bulk chemicals (Figure 1).[19–21] This review aims to delve deeper into organic oxidation while limiting its relevance to OER-mimic conditions.

Oxidation of organic compounds, including alcohols, carbonyl compounds, and amines, is crucial for generating synthons essential for the chemical, pharmaceutical, agrochemical, and material industries.[20,22–25] Moreover, oxidative conversion of renewable feedstocks, for example, biomass-derived hydroxymethylfurfural (HMF) and glycerol is of increasing importance.[22–25] However, the classical chemical oxidation of organic compounds involves higher valent chromium, manganese, copper-oxo compounds, lead salts, activated dimethyl sulfoxide, iodine, organic aminoxyls, etc.[23,26] These approaches pose significant drawbacks, being either toxic (except for manganese-containing

catalysts), limited to small-scale reactions, or plagued by challenges in product yield and isolation, rendering them less reliable for industrial-scale operations. Compared to these, oxidative transformations, using molecular oxygen or air offer significant advantages due to the abundance of inexpensive oxidants, producing water as the by-product during oxidations. In stark contrast, electrochemical energy emerges as a more efficient alternative and sustainable approach, enabling the oxidation of organic molecules without the need for additional expensive, or toxic oxidants. The superiority of electrochemical processes was already been emphasized in the 2018 report from the American Chemical Society (ACS) Green Chemistry Institute Pharmaceutical Roundtable Meeting.[27] The electrooxidation processes can be controlled with high accuracy in terms of product yield and selectivity just by tuning the operating potentials, electrode materials, cell configuration, electrolytes, and more. Additionally, most of the electrooxidations are performed at room temperature and atmospheric pressure,[28–31] presenting a notable advantage over traditional chemical oxidation methods.

The classical electrochemical oxidation of alcohols or amines requires a homogeneous redox mediator, such as 2,2,6,6-tetramethylpiperidin-*N*-oxyl (TEMPO), or its derivative, in conjunction with suitable additives.[32–35] Noteworthy aspect is its versatility across a wide range of solvents, thereby expanding the substrate scope. However, the redox active species exhibits limited stability under prolonged reaction times, presenting challenges in product isolation and purification.[36,37] This challenge can be effectively addressed by employing anodically wired heterogeneous electrode materials with suitable redox features. This approach eliminates the need for catalyst-to-product mixing thus introducing a low-cost separation technique. Interestingly, with a modified cell configuration, a paired electrolysis can be achieved that successfully isolates the anode and cathode processes. The milder operating conditions in organic oxidation reaction (OOR) contribute to enhanced catalyst and electrolyte stability, thus minimizing potential safety hazards associated with it. Moreover, the selectivity of OORs, coupled with lower energy requirements and compatibility with various feedstocks, makes them a scientifically sound and promising choice as an anodic reaction combined with desirable cathode reactions like hydrogen production, CO_2, N_2 or even other organic reduction reactions (ORRs). This approach not only overcomes the limitations associated with homogeneous redox mediators but also enhances the efficiency and selectivity of the electrochemical oxidation process.[31,38]

Nickel is widely known as a ubiquitous element in electrocatalysis owing to its abundance, low cost, and remarkable stability, exhibited by its catalytic component across various reaction conditions.[39–42] Under the alkaline medium, Ni-containing materials irreversibly transform into hydrated oxides with complex phase and electronic structures.[6,7,43–45] These oxides, in turn, can generate redox active species crucial for various electrooxidation reactions. It is important to note that, Ni being a well-known anode material for industrial water splitting, has attracted tremendous interest in OORs. The kinetics for water and organic oxidation are competitive and occur within a close potential range.[6,17,43–46] However, the dynamic nature of the redox behavior and active phase components could differ substantially. While several studies have explored the nature of OOR, its conversion efficiency, and product formation selectivity, a limited number have delved into the active catalyst phase including its redox behavior during OOR.[47] To the best of our knowledge, no review article has comprehensively addressed the nickel-containing active catalytic phase, its redox behavior, and its role in OOR.

In this review, we first discuss the fundamental principles of OOR from both an electron transfer and molecular energy standpoint. Subsequently, a detailed exploration of the stepwise mechanistic pathways involved in diverse OOR processes is presented, with a focus on catalysts based on Ni. The next section delves into the dynamic redox behavior of Ni-based catalysts, providing detailed insights into the probing of Ni's valence states under OOR conditions. Further, we investigate the intriguing phenomena of phase transformation and catalyst reconstruction in Ni-based catalysts, analyzing their profound effects on the control of activity and product selectivity in various OOR scenarios. Finally, we shine a light on the future challenges and opportunities intrinsic to the utilization of Ni-based catalysts in the field of OOR, offering a forward-looking perspective on advancements in this area of electrocatalysis. The central theme of the review is depicted in **Figure 2**. We anticipate that this review will offer a thorough understanding of the crucial aspects of OOR, and this knowledge is deemed essential, especially when considering its potential coupling with hydrogen production or other significant cathodic processes.[48]

2. Mechanism for Organic Oxidation and the Effects of Reactant Hydrophilicity

2.1. General Principle for Organic Oxidation

Electrochemical oxidation of organic compounds can proceed via different pathways depending on the experimental conditions, but in all of them, because of the electron transfer, the original molecule (RA) converts into a reactive intermediate, thereby forming the desired product (**Figure 3**). Generally, at the anode, upon applying voltage, the electron from the highest occupied molecular orbital (HOMO) of the molecule is removed to form a radical cationic species ($RA^{\bullet+}$). This reaction intermediate is highly prone to various reactions such as nucleophilic substitution, dimerization, or the elimination of functional groups (or atoms).

Such a possibility is demonstrated in Figure 3a. During electrooxidation, a more positive potential at the anode leads to a faster reaction. It is important to note that the electron removal process largely controls the product selectivity. If two more different compounds present with closer HOMO energy levels, the possibility of removing electrons from both HOMO levels remains similar, which causes partial transformation or unselective product formation. In this case, suitable functionalization of the substrate can alter the HOMO level thus helping to oxidize at less operating potential and formation of selective product (Figure 3b).[49] Therefore, the energy level position (and the voltage range) where the electron transfer should occur needs to be carefully considered. It is also important to stress that the redox potential of the anode materials has to closely comply with the electron transfer potential of organic reactants. Since it is almost

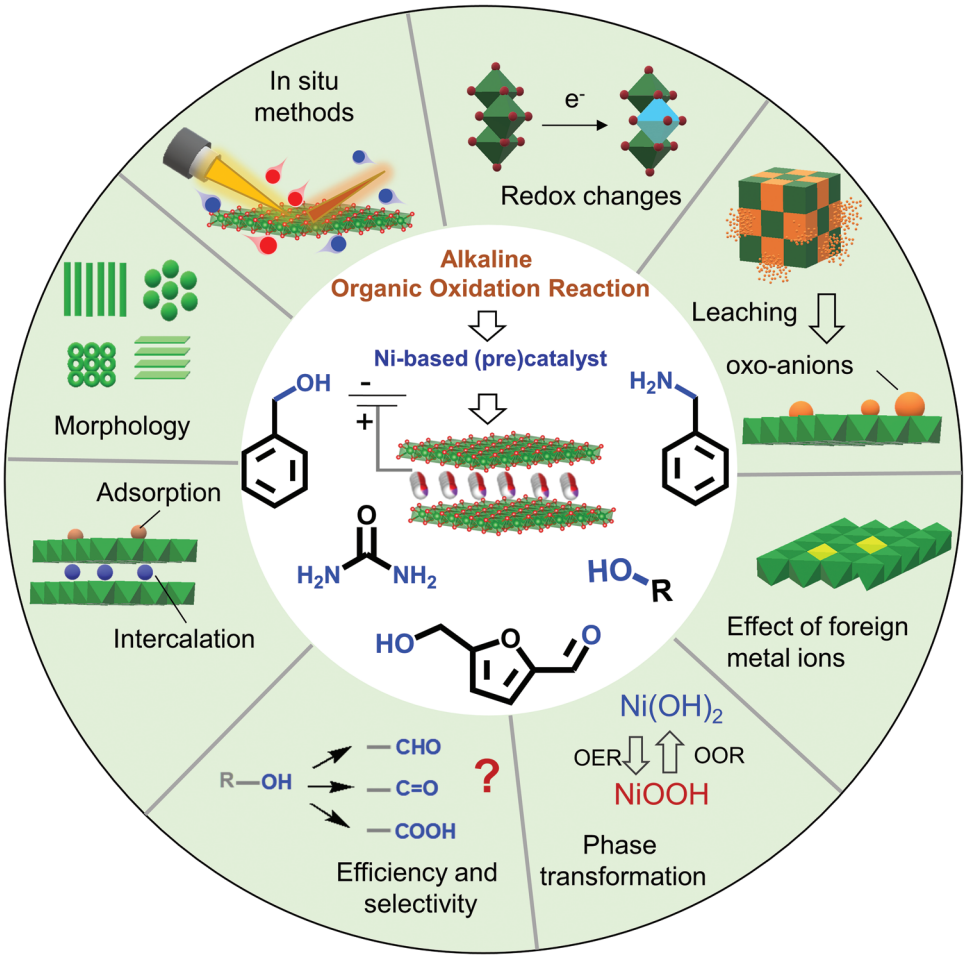

Figure 2. A schematic illustration of the central theme of the review including different dynamic behaviors of Ni-based (pre)catalysts, and utilization of operando studies during the alkaline OOR.

impossible to identify the nature of the chemical reactions from the voltage-current response, one needs to optimize the yield of the desired compound by careful monitoring of the electrochemical conditions including electrochemical cells, electrolytes, and mass transportations.[50–52]

2.2. Mechanism of Different Oxidation Processes

In the alkaline environment, the OER can occur through either an adsorbate evolution mechanism (AEM) or a lattice oxygen evolution mechanism (LOM), involving a four-electron

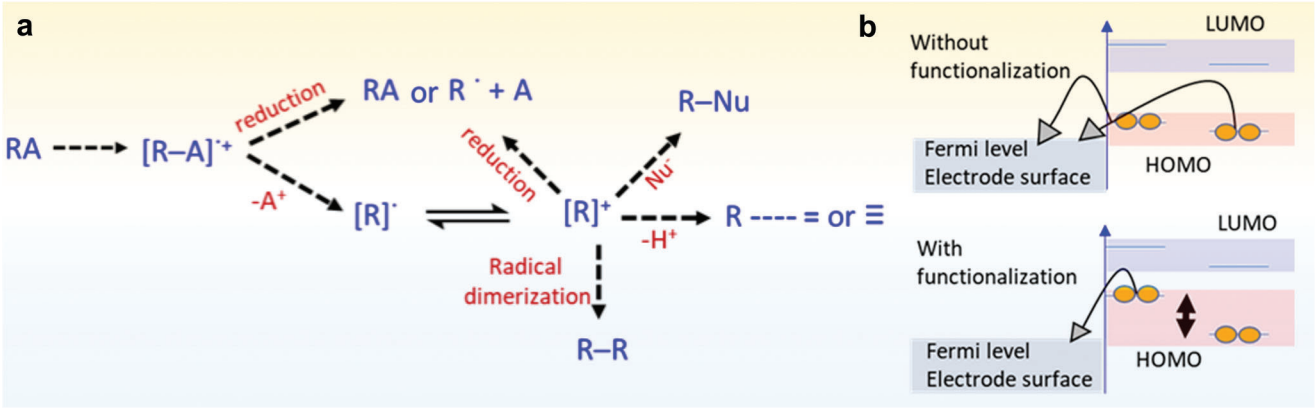

Figure 3. a) Possible pathway for the different OOR. b) Electron transfer pathway for selective and nonselective product formations.

transfer process. Prior to the gaseous oxygen release, the formation and conversion of reaction intermediates follow the sequence: $OH^*\rightarrow O^*\rightarrow OOH^*\rightarrow O_2$.[53] Subsequently, the metal is oxidized into a hydrated oxide commonly known as (oxy)hydroxide (MOOH), which typically acts as an active site/species for OER. In contrast, OOR reactions proceed via diverse mechanistic pathways depending on the organic substrate. Nevertheless, based on a thorough literature search, we limited our discussion only to alcohol, aldehyde, and amine oxidation reactions. Further, we have also discussed the electrooxidation of two special classes of molecules, namely HMF, and urea, which are among the most studied OOR so far.[54]

2.2.1. Oxidation of Amines and Alcohols

Amine and alcohol oxidation undergoes a 4-electron dehydrogenation process, leading to the conversion of amines to nitriles and alcohols to carboxylic acids. Within the area of alcohol oxidation reactions, the scientific community has extensively investigated the intricacies of methanol oxidation (MOR), ethanol oxidation (EOR), n-propyl alcohol oxidation (POR), and benzyl alcohol oxidation (BAlOR). Similarly, among amines, there is notable research on propylamine oxidation (PAmOR) and benzylamine oxidation (BAmOR) specifically employing nickel (Ni)-based catalysts. During this process, MOOH reversibly forms low-valent metal oxide species and simultaneously oxidizes the organic molecules. This mechanism can proceed via either hydrogen atom transfer (HAT) or hydride (H^-) transfer pathway (**Figure 4**). Typically, HAT is a chemical process rather than an electrochemical process, which is commonly referred to as the "indirect oxidation" (ID) process. Alternatively, the reaction mechanism can also proceed via potential dependent (PD) pathways through the hydride transfer route. In the initial step, both amine and alcohol adsorbed on the catalyst surface. In the consecutive step, in the case of amines, a neutral intermediate ($RCHNH_{ads}$) is formed from a negatively charged species ($RCH_2NH^-_{ads}$) after hydride transfer. However, if it follows the HAT mechanism, a radical intermediate is ($R\dot{C}HNH_{ads}$) formed before further oxidizing to nitrile. On the other hand, during alcohol oxidation similar radical species ($R\dot{C}HOH_{ads}$) are formed in the HAT mechanism, while the hydride transfer directly occurs from the α–C of alcohol, before oxidizing to carboxylic acid. At the end of both processes, $M(OH)_2$ is regenerated, completing the catalytic cycle.[55]

2.2.2. Aldehydes Oxidation

Electrochemical aldehyde oxidation is not widely explored. The notable pathway for such an oxidation is through a 2-electron hydroxylation process to produce carboxylic acid. The reaction is initiated via a nucleophilic attack by OH^- ion thus forming a 1,1-geminal diol species, which further oxidizes to corresponding carboxylic acid.[55,56]

2.2.3. HMF Oxidation

HMF is one of the extensively studied organic substrates, which constitutes an aldehyde and alcohol group with a furan backbone. The electrochemical HMF oxidation reaction (HMFOR) to 2,5-furan dicarboxylic acid (FDCA) involves oxidizing an alcohol and an aldehyde group, with two primary pathways (Path I and Path II) depending on the electrolyte pH.

In path I, the oxidation of HMF's alcohol group initiates the process, forming diformylfuran (DFF) as the initial intermediate. Conversely, Path II commences with the oxidation of HMF's aldehyde group, resulting in the formation of 5-hydroxymethyl-2-furancarboxylic acid (HMFCA) as the first intermediate. Both DFF and HMFCA undergo successive oxidation steps, ultimately producing 5-formyl-2-furancarboxylic acid (FFCA) and FDCA. Path II is favored under strongly alkaline conditions (pH $\geq$ 13), while Path I is the primary route in weak alkaline environments (pH < 13) (Figure 4).[57]

It is worth noting here that, in a strong base (when the base-to-HMF ratio of 2 or more), HMF decomposes without forming the desired oxidation products.[58] When the pH is high (above 11), HMF degrades, forming levulinic acid and formic acid (or formate).[59] Additionally, the Cannizzaro reaction occurs, leading to the formation of HMFCA and 2,5-bis(hydroxymethyl)furan (BHMF) through the base-induced transformation of HMF's aldehyde group. This indicates that the pH of the solution is crucial for the HMFOR process, while it is usually recommended to keep the pH value at 8.[60]

2.2.4. Urea Oxidation

Urea oxidation reaction (UOR) is a 6-electron process and generally proceeds via AEM and LOM (Figure 4). These pathways are predicted based on product formation. In the AEM, urea is adsorbed on the catalyst surface (bridge coordination) and the N—H dehydrogenation (4 electron) takes place, which triggers the C—N bond to cleave and N—N coupling to occur. In the next step, *COOH oxidation (2 electron) proceeds through nucleophilic attack by an OH^- ion from solution and finally CO_2 release along with N_2. Among them, the $*CO_2$ desorption step is claimed as the most common rate-determining step (RDS) of UOR. The delay of $*CO_2$ desorption sometimes leads to catalyst deactivation. Importantly, the N–H dehydrogenation may occur at different amino group positions. Thereafter, the intermediate rearrangement steps are required for N—N coupling before complete deprotonation and dehydrogenation of N—H occur. In contrast, LOM proceeds much faster than AEM and involves the lattice oxygen of MOOH species. Upon activation, the catalyst's surface interacts with lattice oxygen, leading to a reaction with intermediates that results in the creation of oxygen vacancies during the UOR. In the subsequent step, OH^- from the electrolyte combines with these oxygen vacancies, forming a new lattice of oxygen and thereby completing a UOR cycle and resulting in N_2 and H_2O as products. Nonetheless, some by-products, such as NO_3^- and NO_2^-, etc may be generated due to the preferential C—N cleavage and OH^- attack during the UOR. Most importantly, the presence of secondary metal (like Fe), a higher concentration of urea, or the vacancy in the system could alter the reaction mechanism.[61]

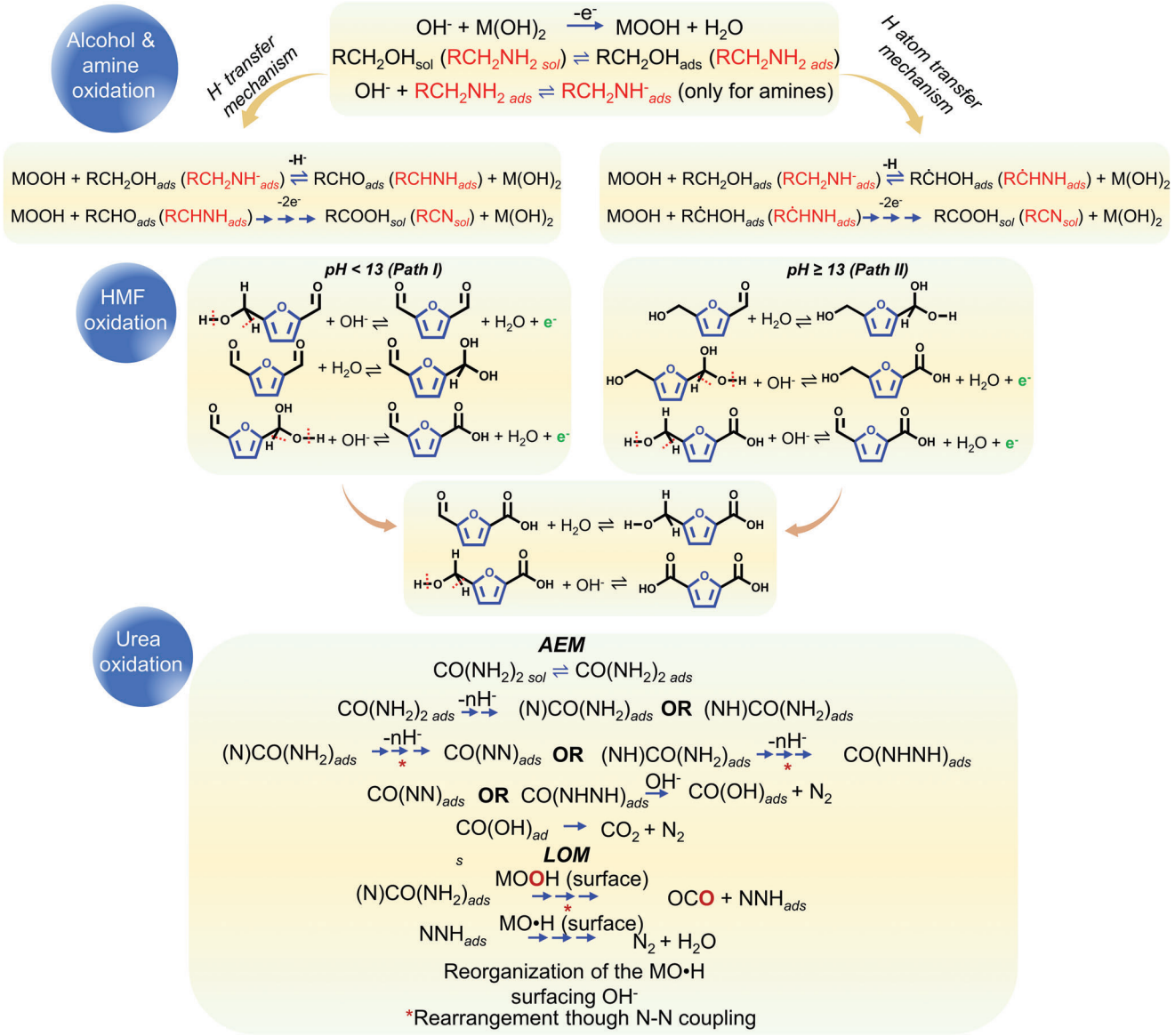

Figure 4. Schematic representation of the mechanistic pathway and the related intermediates for the catalytic conversion of alcohol, amine, HMF, and urea. In general alcohol and amine oxidation either can go via hydride transfer or hydrogen transfer mechanism to produce carboxylic acid/nitrile after complete oxidation. The oxidation of HMF is a pH-dependent process, where the intermediates can be varied depending on the pH value of the electrolyte. However, both pathways lead to the formation of FDCA after a complete charge pass. On the other hand, the UOR occurs majorly via AEM and LOM. These mechanistic pathways were predicted based on product formation.

2.3. Impact of Reactant Hydrophilicity on OOR

The hydrophilicity of organic reactants and their corresponding products showed a noticeable influence on the activity expression of catalysts, particularly within the domain of aqueous environments.

2.3.1. Mass Transport Phenomena

Hydrophilicity dictates the transport kinetics of reactants and products to and from the catalytic surface. Notably, the discriminating affinity of hydrophilic species toward the aqueous phase facilitates their facile migration toward the catalyst, thereby ensuring a steady flow of reactants toward the active sites.[62] These transport dynamics substantiate enhanced reaction kinetics by maintaining an optimal supply of reactants and facilitating the expeditious removal of reaction products.[63]

2.3.2. Surface Interactions

The hydrophilic nature of reactants and products deeply influences their interactions with the catalyst surface. Such species,

owing to their intrinsic propensity for aqueous solvation, tend to exhibit enhanced wetting characteristics upon the catalyst surface, thereby producing improved interfacial contact.[64] This augmented contact augurs well for efficient adsorption and subsequent catalytic transformation.

2.3.3. Interface Electrochemistry

Within the domain of electrochemical reactions, the hydrophilicity of species interfacing with the electrode-electrolyte interface significantly modulates the electrochemical site.[65] This modulation stems from alterations in the double-layer structure induced by hydrophilic entities, thereby enhancing the accessibility of reactants to the electrode surface and, concomitantly, increasing the electrocatalytic activity.[66,67]

2.3.4. Reaction Kinetics

Hydrophilic species may partake in altered reaction mechanisms vis-à-vis their hydrophobic counterparts. The presence of water molecules, ubiquitous within aqueous environments, may cause competition with organic reactants for adsorption sites on the catalytic surface, thus imparting a minute effect on the reaction kinetics and pathways.

2.3.5. Desorption Dynamics

The hydrophilic character of products may substantively influence their desorption kinetics from the catalyst surface. Notably, highly hydrophilic products may evince stronger affinities toward the catalytic surface, thereby impeding their facile desorption and potentially precipitating product inhibition phenomena.[64]

3. Dynamic Behavior of Ni Valence State

The structure-activity/selectivity relationship and the efficacy of OORs are strongly correlated with the oxidation state and/or redox behavior of the catalytically active metal sites. Since the discovery of nickel-based electrodes in electrocatalysis, researchers have diligently pursued an understanding of the evolving oxidation state and local electronic structure during reactions. This investigation has been conducted mainly through various analytical methods, including mainly electrochemical techniques,[68–72] and in situ spectroscopic techniques such as X-ray absorption spectroscopy (XAS) and Raman spectroscopy or quasi in situ X-ray photoelectron spectroscopy (XPS).[73,74] This section aims to elucidate the dynamic redox behavior of nickel and its precise detection, which is crucial in optimizing the performance and selectivity of OORs.

3.1. Electrochemical Redox Behavior of Ni in Oxidation Potentials

3.1.1. In the Absence of Organic Substrates in Alkaline Media

Extensive research has been devoted to comprehensively investigating the electrochemical behavior of Ni in an alkaline solution (without organic substrates) within the oxidizing potential range.[72,75] By looking at the cyclic voltammetry (CV) of the Ni electrode, the effective potential range can be divided into two regions: "low-potential" (−0.2 to 0.5 V vs RHE) where Ni can be oxidized and reduced reversibly, and the "high-potential" (0.5 to 1.6 V vs RHE) with irreversible Ni-oxo species formation. Below $E = 0$ V (vs RHE), hydrogen evolves, while above $E \approx 1.5$ V (vs RHE), oxygen evolves. For metallic Ni, the main redox within the low-potential regime involves the genesis of lower valent $Ni(OH)_x$ during the anodic scan.[76] Interestingly, Ni electrodes can form a NiO layer upon contact with oxygen species. This NiO layer can be partially transformed to α-$Ni(OH)_2$ forming a three-layer structure Ni | NiO | α-$Ni(OH)_2$).[76,77] In the high-potential window, α-$Ni(OH)_2$ is transformed to β-$Ni(OH)_2$ irreversibly with concomitant generation and/or increment of NiO layer as the potential increases from 0.5 to 1.2 V (vs RHE).[78–80] The formation of β-$Ni(OH)_2$ layer brings a reduction of the cathodic peak within the low-potential region followed by the gradual shift of the peak toward increasingly negative potential (**Figure 5**a). As the potential increases beyond 1.2 V (vs RHE), the α/β-$Ni(OH)_2$ transformed into γ/β-NiOOH. This is typically visible by the anodic peak at 1.4 V (vs RHE). At more higher potential (>1.5 V), the surface of the Ni-electrode is covered with high valent (Ni^{3+} mostly) $Ni(OH)_x$ species, as proved by different spectroscopic techniques particularly using in situ Raman spectroscopy.[81,82] The in situ-formed NiOOH is a non-stoichiometric oxide. Its property and OOR activity largely depend on the nature (chemical and solid-state structure, morphology, etc.) of the (pre)catalysts.[69,75]

3.1.2. In the Presence of Organic Substrates in Alkaline Media

Electrochemical OOR on Ni-based catalyst or NiOOH surface in the presence of organics can be elucidated through two distinct mechanistic pathways, as previously discussed.[72,83,84] The classical Fleischmann's mechanism proposed in the 1970s, highlights the coupling between the oxidation of organic compounds and the redox reaction involving $Ni(OH)_2$/NiOOH. In this mechanism, the redox couple $Ni(OH)_2$/NiOOH functions as a redox mediator, capable of generating NiOOH, facilitating the OOR.[85] In the case of alcohols, the RDS is the chemical oxidation of the adsorbed reactant via HAT (see Figure 3) to generate the carbon-centered radical. During this process, NiOOH gets reduced back to the $Ni(OH)_2$ species. In contrast, a recently proposed mechanism through hydride transfer, presented by Choi and Hammes-Schiffer et al., successfully distinguishes subtle differences in potential between the redox peak of $Ni(OH)_2$/NiOOH and the peak corresponding to alcohol oxidation, which occurs at a relatively higher positive potential.[55,72,84] Using experimental and computational analysis, they have quantitatively deconvoluted two distinct pathways of alcohol and aldehyde oxidation reactions. They proposed a new pathway that entails hydride transfer from the organic substrates to the Ni^{4+} active site in NiOOH species during the OOR.[72] The linear sweep voltammogram taken during OOR indicates how the contribution of "indirect" and "potential dependent oxidation" drastically differ depending on the molecular structure of the organic substrate, as indicated in Figure 5b–d. In the absence of an organic substrate, a peak

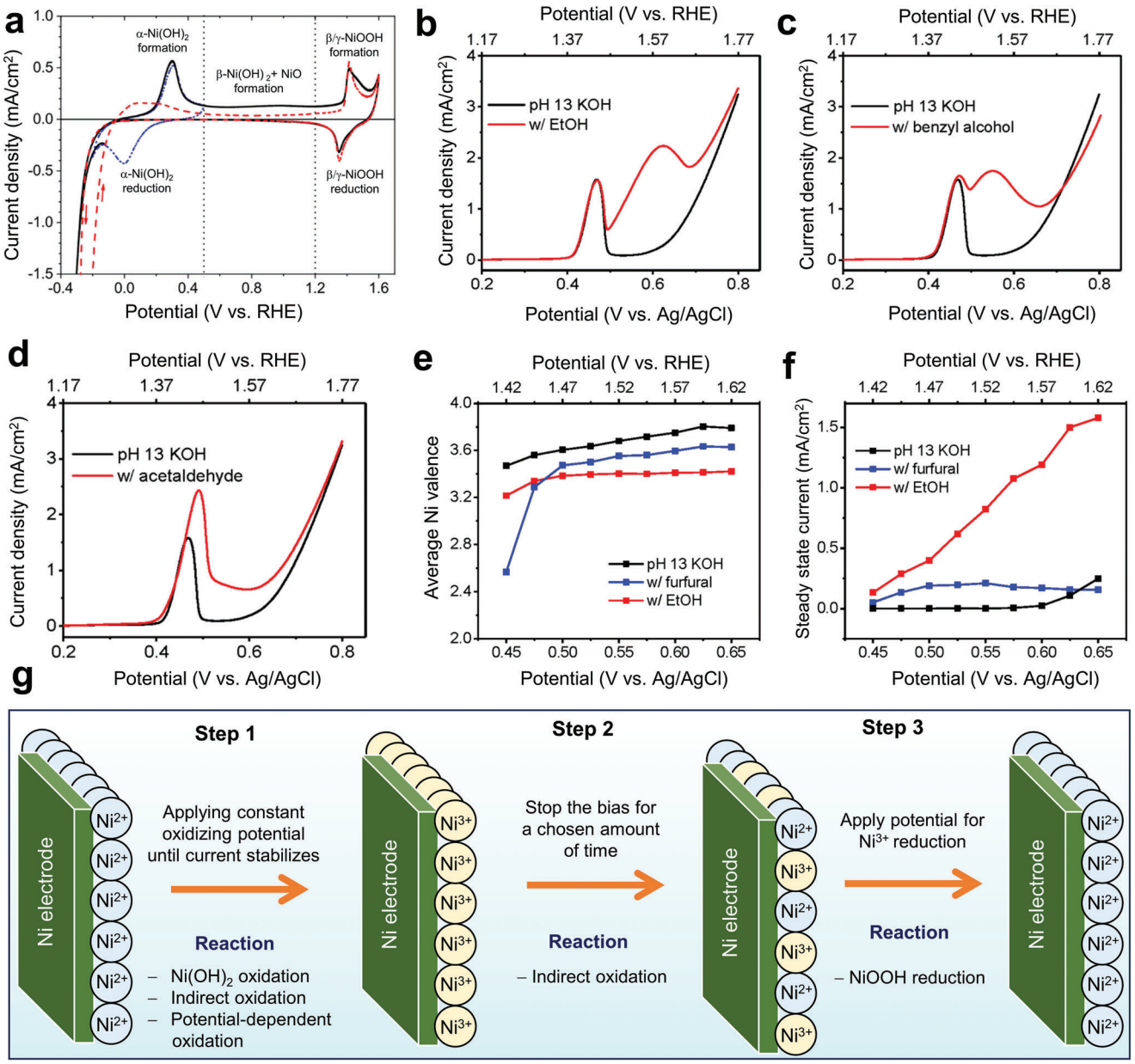

Figure 5. a) Cyclic voltammograms (CVs) of a polycrystalline Ni electrode are presented in N_2-saturated 0.1 M NaOH at a sweep rate of 50 mV s^{-1} and a temperature of 25 °C. The CV is indicated by a dash-dotted blue curve, encompassing the potential range from −0.2 to 0.5 V versus RHE. Additionally, two other CVs with the first scan represented by a solid black curve and the second scan by a dashed red curve, covering the potential range from −0.3 to 1.6 V (vs RHE). Reproduced with permission.[17] Copyright 2020, American Chemical Society. LSVs of $Ni(OH)_2$ electrode in a pH 13 electrolyte with b) 10 mM ethanol, c) 10 mM benzyl alcohol, and d) 10 mM acetaldehyde. e) The potential dependent average Ni valence under steady-state conditions in a stirred solution of pH 13 without (black), with 10 mM furfural (blue), and, 200 mM EtOH (red). f) Steady-state current density values at pH 13 in the absence (black), in the presence of 10 mM furfural (blue), and 200 mM EtOH (red). g) Schematic illustration of the three-step rate deconvolution process where the oxidized Ni catalyst is represented with Ni^{3+} sites. However, Ni^{4+} is also present in the electrode which is neglected to simplify the demonstration. Reproduced with permission.[72] Copyright 2020, American Chemical Society.

at ≈1.37 V versus RHE illustrates the conversion of $Ni(OH)_2$ to NiOOH, followed by a water oxidation wave. Generally, in OOR, the reduction of the Ni^{3+} state to Ni^{2+} is associated with the proton-coupled electron transfer (PCET), and identified as the RDS. In the presence of acetaldehyde (the red line in Figure 5d), an increased conversion of $Ni(OH)_2$ to NiOOH occurs during the potential sweep, aligning with Fleischman et al. proposed mechanism. In contrast, the oxidation of ethanol and benzyl alcohol (the red line in Figure 5b,c), exhibits minimal enhancement in $Ni(OH)_2$/NiOOH peak. Instead, a new anodic peak at a more positive applied bias is observed, which is attributed to the potential-dependent oxidation mechanism distinct from Fleischmann's potential-independent "indirect oxidation."[85]

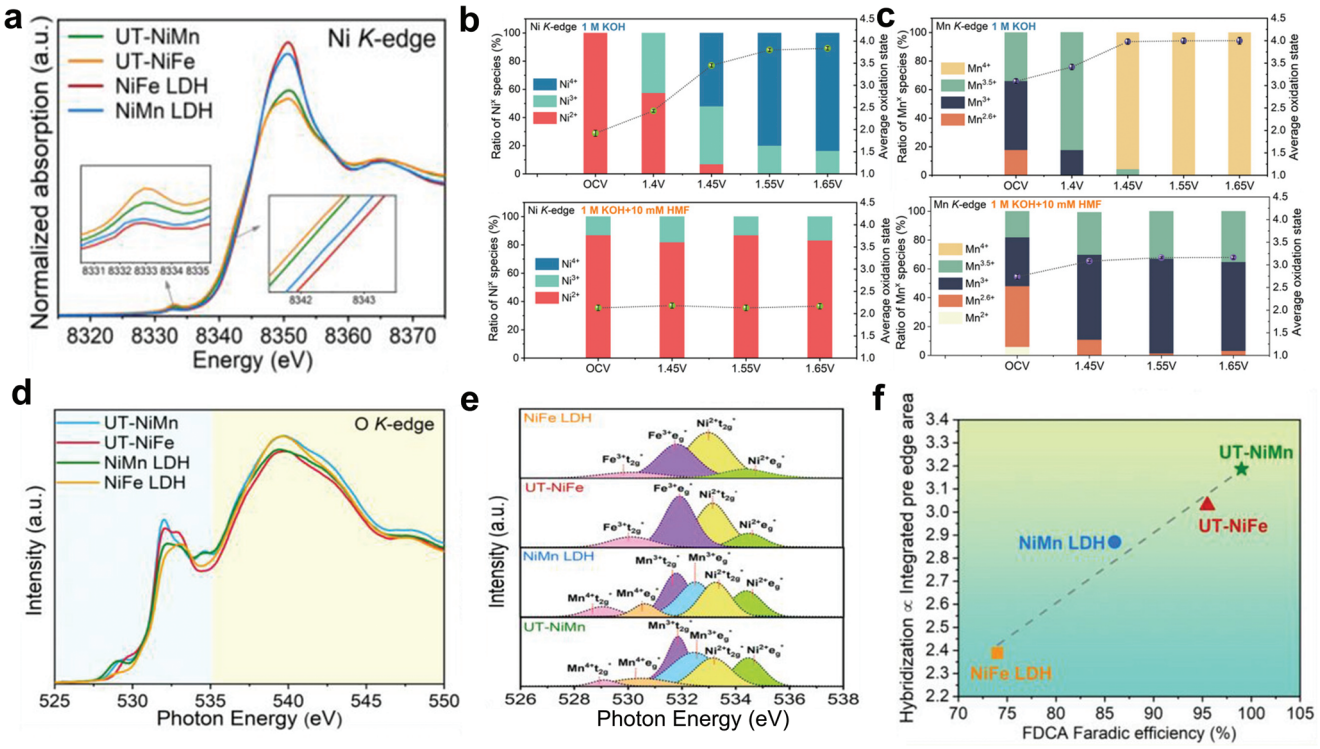

Figure 6. a) Ni K-edge XANES different Ni-based catalysts. Comparison of the various b) Ni species and c) Mn species having different oxidation states determined from optimal linear combination fitting of the XANES spectra in 1 M KOH in operando conditions. d) NEXAFS spectra for O K-edge of UT-NiMn, NiMn LDH, UT-NiFe, and NiFe LDH, and e) the fitted pre-edge signature of the O K-edge. f) The plot of covalence/hybridization level of various Ni-derived catalysts and their selectivity toward FDCA. Reproduced with permission.[89] Copyright 2023, Wiley-VCH.

3.2. Determination of Oxidation State in Ni-Based Catalyst Utilized for OORs

The study on electrochemical OOR suggests that the catalytic onset potential for the alcohol oxidations is predominantly governed by the favorable oxidation state of the electrocatalyst rather than their inherent thermodynamics, distinguishing it from numerous molecular electrocatalysts.[86] Consequently, the determination of oxidation state has paramount importance in the context of OOR. As discussed in the previous section, the basic understanding of the change in the Ni oxidation state can be estimated from the nature of the CV cycle in the OOR process. Choi and co-workers introduced a three-step redox-based electrochemical procedure to identify the oxidation state of Ni, along with the rates of both the potential-dependent and "indirect" mechanisms. Figure 5e illustrates a comparison of average Ni valence during the "indirect oxidation of furfural," PD oxidation of ethanol, and water as a function of applied potential. The steady-state current under stirring at each applied potential reveals a linear increase in the average Ni oxidation state from +3.47 to ≈+3.8 at 0.625 V versus Ag/AgCl at pH 13 (in KOH), attributed to the accumulation of Ni^{4+} sites with increasing potential, followed by a plateau due to enhance rate of Ni^{4+} consumption during water oxidation. In this way, the average oxidation state of Ni in NiOOH can be estimated with the help of modifying the deconvolution technique as presented in Figure 5g. The obtained results on the Ni valence in this process align well with findings from in situ XAS and other analytical techniques like Raman spectroscopy or quasi in situ XPS spectra.[72]

Operando X-ray absorption near-edge structure (XANES) measurements have been extremely helpful in mapping the oxidation state of Ni in the real-time OOR. The oxidation state can be estimated by analyzing features near the absorption edge in the XANES spectra, considering factors such as edge position, white line intensity, spectral shape, and comparisons with reference standards.[87,88] Bedford and co-workers have investigated the HMFOR activity of ultra-thin (UT)-layered double hydroxides (LDH), where they found that the electron-rich Ni site originating from oxygen defects is responsible for the catalysis (**Figure 6a**).[89] The in situ XANES spectra reveal the quantification of oxidation states in UT-NiFe and UT-NiMn. A final oxidation state of Ni was determined as 3.80 and 3.84 in UT-NiFe and UT-NiMn, respectively, at around 1.5 V. Under HMFOR conditions, both UT-LDHs exhibit stabilized Ni^{2+} states, while Fe in UT-NiFe maintains an oxidation state of 2.88. Notably, Mn in UT-NiMn displays an increased oxidation state even in the presence of HMF, suggesting a higher rate of catalyst deprotonation, resulting in a larger working window and higher selectivity toward HMFOR compared to UT-NiFe (Figure 6b,c). They have also employed near-edge EXAFS to investigate the origin of improved activity and the increased deprotonation propensity of UT-LDHs. The XAS of O *K*-edge provides insight into the catalyst performance, ideas about the Ni valence state, and the metal-O hybridization level.

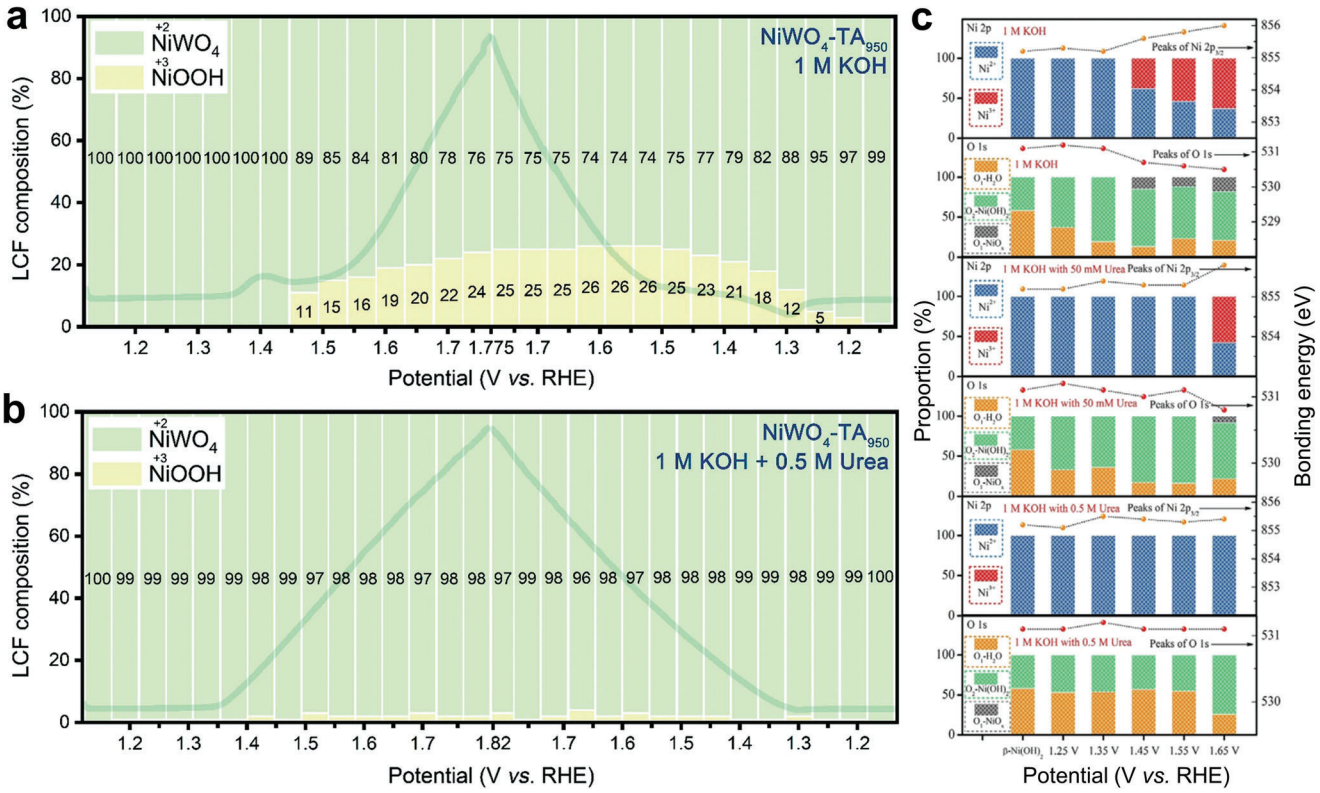

Figure 7. In situ tracking of the Ni oxidation state in $NiWO_4$-TA 950 during oxidation of the water and urea. Linear combination fitting (LCF) outcomes from Ni K-edge XANES spectra under operando condition in a) 1 M KOH and 1 M KOH + 0.5 M urea. The shaded lines represent the respective LSVs without *iR*-correction in the background. Reproduced with permission.[90] Copyright 2022, Royal Society of Chemistry. c) Quasi in situ XPS analysis of β-$Ni(OH)_2$ electrode in 1 M KOH with varied concentrations of urea (0, 50, and 500 mM). Reproduced with permission.[91] Copyright 2021, Wiley-VCH.

The decrease in intensity at t_{2g} peaks in the Ni^{2+} spectra of UT-LDHs and the corresponding increase in the intensity at t_{2g}* feature in the O *K*-pre-edge region. This indicates the lowering of the oxidation state of Ni and charge transfer phenomena from O to Ni site (Figure 6d–f). This kind of enhanced metal (M) $3_{d\text{-}O}$ 2p hybridization in UT-LDHs correlates strongly with improved HMFOR to FDCA. Additionally, strong hybridization induces a shift from antiferromagnetic to ferromagnetic ground states, particularly evident in UT-NiMn enhancing electrical conductivity and charge transfer ability in UT-LDHs compared to no-UT materials.[89]

Using XANES, Lin et al. also investigated the role of Ni^{3+} in both OER and UOR in $NiWO_4$-based catalysts. In KOH, during OER, accumulation of Ni^{3+} initiates at ≈1.45 V (vs RHE) and remains high (≈20%) at higher voltages. This observation implies a higher rate of Ni^{3+} formation than its consumption during OER (**Figure** 7a). In the presence of urea, the accumulated unoccupied Ni^{3+} sites (from the OER intermediate) catalyze the UOR, preventing a current collapse in the OER zone, as evidenced by nearly negligible Ni^{3+} signals throughout the urea oxidation scan (Figure 7b).[90] Interestingly, Chen et al. utilized quasi in situ XPS to analyze the oxidation state of Ni, as well as O in β-$Ni(OH)_2$ as mentioned in Figure 7c. They found that the higher binding energy in complex $Ni_{2+d}O_xH_y$ species (such as a mix of NiOOH and NiO_x) corresponds to the higher oxidation state of Ni. As a consequence, a lower bonding energy is observed in the case of Ni—O bond in O 1s spectra. This study reveals the oxidation state of Ni evolves at different concentrations of urea in an oxidation reaction environment.[91] Similarly, Yang et al. reported the correlation between the oxidation state of Ni in several (pre)catalysts, using ex situ XPS, and associated it with the onset potential of HMFOR.[92] It was observed that the oxidation state of Ni is higher in Co-$Ni(OH)_2$ compared to Fe-$Ni(OH)_2$. Interestingly Co-$Ni(OH)_2$ exhibited a lower onset potential (1.32 V) compared to Fe-$Ni(OH)_2$ (1.39 V).

Another powerful technique to probe the oxidation state of Ni during OOR is in situ Raman spectroscopy. So far, the oxidation state, as well as the coordination of the Ni site in NiOOH, has been modified by the use of different metalloids (NiP_x, NiS_x, and $NiSe_x$), leading to the formation of oxyanion-coordinated amorphous NiOOH, as characterized by in situ Raman spectroscopy (**Figure** 8a).[93] Among them, NiOOH-PO_X has been found to have an optimal local coordination environment and accelerates the electrocatalytic activity of Ni sites toward selective oxidation of methanol to formate (Figure 8b).

In this particular case, the in situ Raman was employed to delve into the low-frequency interface. The Raman spectra unveiled two distinguishable peaks 474 and 551 cm^{-1} correspond to the bending ($d_{Ni—O}$) and stretching ($n_{Ni—O}$) modes of Ni^{3+}-O, respectively. Beyond 1.42 V, the electrooxidation potential of NiP_x-R reveals Ni^{3+}-O in the oxide layer (Ni^{2+}-O_xH_y) during OER, while δ(Ni—O) emerges after 1.32 V in MOR, suggesting the

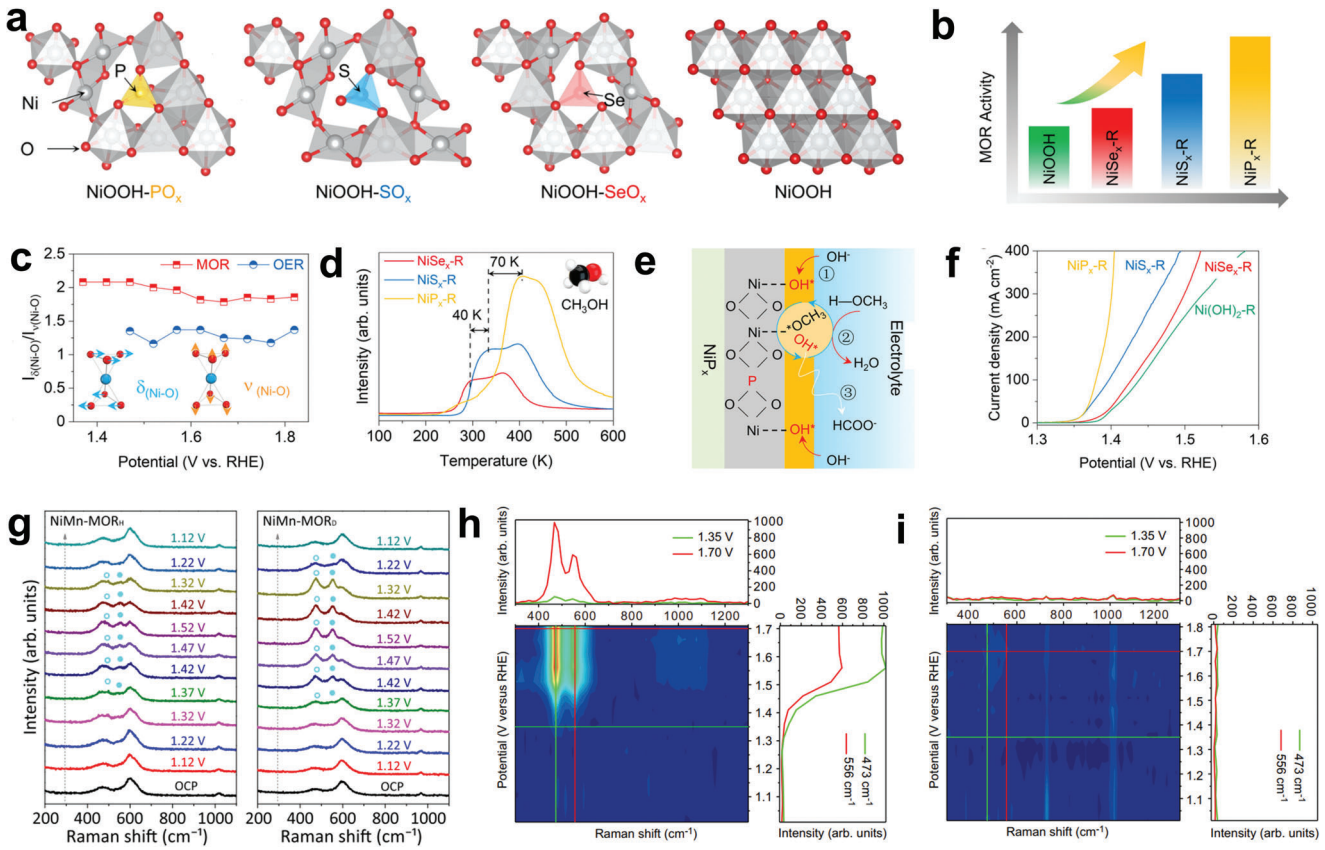

Figure 8. a) Optimized structural model for the oxyanion-modified NiOOH and the pristine NiOOH. b) The trend of electrochemical MOR activity in different oxyanion-modified NiOOH catalysts. c) The ratio of $\delta_{(Ni-O)}$-to-$\nu_{(Ni-O)}$ in the operando Raman spectroscopic study in the operating potentials. d) Temperature-programmed desorption curves for different oxyanion-modified NiOOH for methanol molecules. e) Schematic representation of the MOR mechanism on NiP$_x$. f) Polarization curve of oxyanion-modified NiOOH in MOR condition. Reproduced with permission.[93] Copyright 2022, Nature. g) In situ Raman spectra of NiMn-LDHs were studied at various potentials under MOR conditions using CH_3OH/H_2O or CD_3OD/D_2O solutions. The blue circles denote the bands corresponding to Ni^{3+}-OOH. Reproduced with permission.[73] Copyright 2023, Nature. Operando Raman spectra of nickel boride sample during h) OER and i) MOR process. Reproduced with permission.[94] Copyright 2022.

oxidation of $Ni(OH)_2$ into NiOOH, establishing NiOOH as the primary MOR catalyst. The pronounced difference in the $I_{\delta/\nu}$ ratio between MOR and OER, as depicted in Figure 8c, highlights the distinct lattice structure of formed NiOOH, with higher $I_{\delta/\nu}$ in γ-NiOOH due to its more disorderly and loosely structured β and γ phases.[95,96] The very first step for MOR involves the adsorption of methanol molecules. Temperature programmed desorption (TPD) measurements (Figure 8d) were implemented to investigate the nature of the adsorption of reactant molecule on catalyst surface along with the strength of Ni—O bond and it was found that NiP$_x$-R exhibits a higher desorption temperature (405 K) for methanol compared to NiS$_x$-R (335 K) and NiSe$_x$-R (295 K), establishing a clear correlation between the oxidation state and the stronger methanol adsorption energy (Figure 8e) which, in turn, affect the MOR activity (Figure 8f).[93]

Feng's team found that the Ni^{2+}/Ni^{3+} oxidation in NiMn-LDH is a quasi-irreversible process, which is in stark contrast to the fully reversible characteristics exhibited by NiFe-LDH. Consequently, the introduction of Mn emerges as a crucial factor in facilitating the in situ generation of Ni^{3+}-OOH, which is the key active species for MOR.[73] They have conducted a series of operando Raman measurements to detect the role of Mn in tuning the oxidation state and local environment of Ni in NiOOH. The Ni ions in NiMn-LDH undergo a shuttle mechanism, transitioning between Ni^{2+} and Ni^{3+} states during the catalysis of the MOR. Concurrently, the Mn^{3+}-O band, located at 600 cm^{-1}, remains constant across the entire potential sweep. This consistent observation suggests that the redox transition does not involve the Mn ions within the NiMn-LDH structure. From the operando Raman measurement in a deuterated solvent, they proved the transient and limited formation of NiOOH in NiMn in optimal MOR conditions (Figure 8g). Similar bending vibration and stretching vibration of Ni^{3+}-O of γ-NiOOH was observed at ≈473 and ≈556 cm^{-1} at 1.35 V in the case of the nickel boride catalyst.[94] Additionally, they have also detected the broadband in the 800–1150 cm^{-1} wavenumber due to the formation of $NiOO^-$ (Figure 8h).[94,97,98] Nevertheless, in the process of MOR conditions, there are no characteristic peaks observed in the operando Raman spectra, which indicates that the phase transformation or the oxidation of Ni^{2+} does not occur in the presence of a higher concentration of methanol.

UV–vis absorption spectroscopy is also employed in electrocatalysis to understand the oxidation state of metals crucial to

various electrocatalytic reactions.[117] By analyzing electronic transitions in metal sites, such as those in transition metal-derived catalysts used for OER, this technique in the operando condition, contributes essential information for the precise elucidation of the valence state of the metal sites and enhancement of electrocatalytic mechanisms and performance in diverse applications, spanning from fuel cells to water electrolysis.[118–120] It has been also applied in the case of OOR to find the evolution of the metal valence state, especially Ni. Zou and co-workers utilized in situ UV–vis spectroscopy to understand the oxidation state of Ni during UOR within a custom three-electrode cuvette employing the diffuse reflectance model with an integrating sphere. The in situ electrochemical UV–vis absorption spectra revealed the light absorption of Ni^{3+} species at 500 nm, at a higher potential than 1.3 V.[121] These findings undoubtedly suggest that urea undergoes oxidation mediated by Ni^{3+} species.

Various strategies for modulating the oxidation state, electronic structure, and local environment of Ni have been investigated in recent years, particularly through the engineering of secondary elements associated with the precatalysts,[45] such as Fe, Mn, Co, Si, and Ga, as well as the synthesis of Ni-derived compounds such as Ni-based oxides,[114] nitrides,[110,116] hydroxides,[68,73,122] borides,[94,111] chalcogenides,[70,103] pnictides,[43] or Ni-single atom catalysts.[100,106] The major findings of all the previously reported Ni-based catalyst and their application in various OOR processes are depicted in **Table 1**.

The key takeaway from the current chapter is that, with a Ni-containing catalyst, the OOR takes place at a sufficiently high potential, thereby facilitating the accumulation of a higher valent Ni state ($Ni^{3+/4+}$) within the corresponding oxo species. These states promptly drive HAT ("indirect oxidation") or hydride transfer (potential-dependent oxidation) from the organic reactant. Furthermore, it is conceivable that electrophilic active oxygen species originate from the $Ni^{3+/4+}$(oxy)hydroxides, expediting proton abstraction from the organics. Regardless, the outcome is the formation of Ni^{2+}-oxo species. This phenomenon holds true for alcohols, amines, and aldehydes studied thus far, irrespective of their structure. However, the structure plays a crucial role in determining the reaction rate, product selectivity, byproduct formation, and other factors. It is important to note that the OOR is kinetically more challenging than the OER and should occur well before reaching the thermodynamic OER potential (1.23 V). Several reports demonstrate the OOR using Au, Ag, Cu, and glassy carbon occurs well before the OER potential, suggesting that OOR is feasible without relying on higher valent metal-oxo species; rather, suitable surface adsorption and electrical conductivity are sufficient to initiate the process.[2,123–125] In this regard, we tabulated the oxidation state transformation of the Ni-containing catalysts and their corresponding role in the OOR (**Table 2**). Thus, a Ni-containing catalyst, exhibiting dynamic redox behavior and switching its oxidation state, not only facilitates atom transfer or forms high-energy active oxygen species but also serves as a conducting platform to guide the reaction.

In OORs, organic reactants are one-time reagents and are gradually consumed during bulk electrolysis. In such instances, the redox-active Ni^{2+} ions regenerate to form $Ni^{3+/4+}$, which, if not encountering an organic starting material, cannot be quenched back into Ni^{2+}, given that the anodic potential remains operational. Consequently, the limiting current density and hydrogen production rate gradually decrease, particularly with reduced organic reactant concentrations. This phenomenon resembles the degradation of catalytic activity seen with the gradual decomposition of a redox mediator.[126] Nonetheless, the potential-dependent dynamics of $Ni^{2+}/Ni^{3+/4+}$ should persist, behaving as if under similar conditions to the OER.

Of note, all organic reactions are diffusion-controlled, leading to a reorientation of the electrical double layer. Furthermore, there is no guarantee that the Ni-oxo species, with variations in hydration extent, morphology, defects, and short-range order, will remain identical to their preconditioned state.[93,94] Hence, the catalytic activity may exhibit slight variations in subsequent cycles.[124,127–129] However, we believe that the comprehension and extraction of meaningful information regarding the active catalyst phase operational during long-term OOR remain underexplored and warrant substantial attention. As we observe the discernible phase transition of the catalyst materials during the OOR, the need for a thorough and detailed discussion becomes evident. In the following sections, we discuss these parts more comprehensively.

4. Effect of the Apparent Phase Change on the Selectivity and Efficiency of Product Formation

As discussed in the previous chapter, during OOR, the Ni oxidation state changes rapidly and concomitantly affects the phase reconstruction of the metal sites. A comprehensive demonstration by Choi and co-workers elucidated this phenomenon by observing the change in color of the $Ni(OH)_2$ coated electrode under OER and OOR conditions.[108] As-deposited thick film of $Ni(OH)_2$ exhibits an opaque white color and rapidly changes after the first LSV turns opaque brown, indicating bulk oxidation to NiOOH. Following the LSV, the introduction of 5 mM of HMF caused the NiOOH electrode to shift from opaque brown to opaque white, signifying the conversion of NiOOH to $Ni(OH)_2$ due to HMFOR. Similarly, Mu et al. also synthesized $Ni(OH)_2$ and oxidized it under a KOH medium to produce Ni^{3+}OOH, which is analogous to the OER active phase. Interestingly, when this activated electrode (NiOOH) was applied for HMFOR, a reduction of Ni^{3+}-O to Ni^{2+}-O was observed.[92] Additionally, doping of different elements (Fe, Co, Mo, Mn, Cr, Ga) has been also investigated in the same work. They found that Cr-doped $Ni(OH)_2$ performed better compared to other metals due to the facile PECT process (**Figure 9a**). During the in situ Raman study, at a potential of 1.5 V (vs RHE), the $Ni(OH)_2$ was oxidized to NiOOH in the absence of HMF, while in the presence of HMF, the characteristic peaks of Ni^{3+}-O started to weaken and eventually disappeared. Such observation was noticed for Cr-$Ni(OH)_2$ within 3 s after HMF addition, in contrast to 12 s in the case of Mo-$Ni(OH)_2$. This showed that Cr-doping significantly improved the HMFOR activity by facilitating the PECT process.[92] Another work by Ding and colleagues explored this doping phenomenon toward amine oxidation. They prepared a series of transition-metal (TM) doped α-$Ni(OH)_2$ (TM were Mn, Fe, Co, and Cu) and observed that Mn doping enhanced amine adsorption on the intermediate γ-NiOOH while maintaining the ability to adsorption of oxygenated species on the adjoining Ni-sites (Figure 9b). Importantly, NiMn showed the highest activity and selectivity toward amine oxidation and outperformed other monometallic or bi-metallic materials (Figure 9c).[75] Wang et al.

Table 1. Summary of Ni-based catalyst reported for electrochemical OORs.

Catalyst	Electrolyte	Organic substrate	Applied Potential (V vs RHE)	Product selectivity (FE %)	Stability	Findings of the paper (probing the oxidation state)	Refs.
NiB_x@Ni	1 M KOH	1 M methanol	1.61 V	Formate (100%)	24 h at 100 mA cm^{-2}	Operando EIS and Raman to probe the effect of concentration of methanol on phase transition and activity. Features for Ni^{3+}-O of γ-NiOOH were absent during MOR	[94]
NiMn hydroxide	1 M KOH	3 M methanol	1.33/1.41 V	Formate (100%)	20 h at 100 mA cm^{-2}	Probing reversible redox transitions of Ni^{2+}-$(OH)_2$/Ni^{3+}-OOH and a concomitant MOR. Ni^{2+}-$(OH)_2$ is found as the active species in MOR.	[73]
NiOOH-PO_x	1 M KOH	0.5 M methanol	1.4–1.7 V	Formate	1 h at ≈250 mA cm^{-2}	Effect of different oxyanions (TO_x: T = P, S, and Se) on the local coordination of Ni and Ni^{2+} is acting as the active site for MOR.	[93]
β-$Ni(OH)_2$ and NiO	1 M KOH	0.5 M ethanol	1.15–1.30 V	–	–	Nucleophile oxidation reaction NOR originates from β-Ni(OH)O having electrophilic lattice oxygen and $NiO(OH)_{ads}$ containing electrophilic adsorption oxygen.	[99]
Ni–2D–O–SA	1 M KOH	1 M methanol, ethanol, and benzyl alcohol	0.9 V versus Hg/HgO	Respective oxidized product	12 h at 60 mA cm^{-2} for MOR	Molecular engineering strategy of tuning the local environment of Ni for MOR, EOR, and BOR.	[100]
NiOOH	KOH (pH 12–14)	alcohols and aldehydes	1.52 V	Respective oxidized product	–	Understanding of hydrogen atom and hydride transfer mechanism. Ni valence +3.58 for benzaldehyde.	[84]
hp-Ni	1 M KOH	10 mM benzyl alcohol	1.35, 1.5 V	Benzoic acid (97%)	–	Design of low-cost 3D hierarchically porous Ni catalyst.	[69]
NiS_2/CFC	1 M KOH	0.45 M 2-propanol	1.348 V	Acetone (98%)	24 h at >10 mA cm^{-2}	Single-crystalline NiS_2 nanostructure film prepared by vapor-phase hydrothermal (VPH) method. Ni^{3+} species is found to be responsible for alcohol to ketone production	[101]
Fe-NiOOH	1 M KOH	0.05 M benzyl alcohol	1.45–1.60 V	benzaldehyde and benzoate	1 h at 1.6 V (vs RHE)	Effect of Fe incorporation on Ni redox position and the onset of organic oxidation reaction and the role of Ni^{3+}	[102]
NiS-M	1 M KOH	0.1 M HMF, benzylamine, benzyl alcohol	1.49 V	Respective oxidized product	2 h at 1.49V (vs RHE)	Design of efficient NiS (pre)catalyst derived from a novel molecular precursor	[103]
$Ni(OH)_2$-SDS	0.5 M KOH	50 mM cyclohexanone	1.5 V	Adipic acid (93%)	24 h at 0.8 V (cell potential)	The intercalated SDS in $Ni(OH)_2$ facilitates the mass transfer of cyclohexanone and $Ni(OH)_2$ is found to be the active phase	[104]
t-Ni/Co MOF	1 M KOH	Benzylamine	1.30 V	Benzonitrile (73%)	9 h at 10 mA cm^{-2}	Use of MOF-derived catalyst for primary amines into nitriles. Higher valent Ni^{+3} to transformed Ni^{+2} during the reaction	[105]
Ni_2Si/NF	1 M KOH	50 mM benzylamine	1.49 V	Benzylnitrile (99%)	40 min at 1.49V (vs RHE)	Reporting structurally ordered intermetallic (pre)catalyst highly selective for amine oxidation in broad substrate scope.	[45]
Mn-α-$Ni(OH)_2$	1 M KOH	5 mM benzylamine	1.3–1.45 V	Benzylnitrile (96%)	–	Intermediates from partial OER and simultaneous amine oxidation processes are proposed via a bi-adsorption mechanism. The consumption of active $Ni^{3+\delta}$–O^* was identified by BA	[75]
Ni SACs/$Ti_3C_2T_x$	1 M KOH	0.5 M hydrazine	0.1 V	Nitrogen (92.7%)	24 000 s at 0.1 V (vs RHE)	Having ultralow onset potential of only −0.03 V (vs RHE) for OOR.	[106]

(*Continued*)

Table 1. (Continued)

Catalyst	Electrolyte	Organic substrate	Applied Potential (V vs RHE)	Product selectivity (FE %)	Stability	Findings of the paper (probing the oxidation state)	Refs.
Ni_2P/NF	1 M KOH	0.5 M hydrazine	1 V	Hydrazine oxidation	10 h at 100 mA cm^{-2}	High-performance non-noble-metal 3D catalyst electrode for HzOR and hydrazine sensing.	[107]
S-$Ni(OH)_2$	1 M KOH	0.1 M propylamine	1.317 V	Propionitrile (99.5%)	40 h at 1.5V (vs RHE)	Unraveling the role of chalcogen leaching using operando EIS, Raman spectroscopy. Ni^{3+}-OH species have been found in operando Raman spectroscopy	[70]
NiFe-LDH nanosheet	1 M KOH	10 mM HMF	1.33 V	FDCA (98.6%)	13 h at −0.33 V (vs RHE) for HER‖ HMFOR	First report on using bimetallic metal hydroxide/oxide catalyst.	[58]
NiOOH, CoOOH, and FeOOH films	0.1 M KOH	5 mM HMF	1.47–1.71 V	FDCA, DFF, HMFCA, FFCA	4.7 h at 1.47 V (vs RHE)	Methodical comparison of the intrinsic catalytic activity of all metal-OOH.	[108]
Cr-$Ni(OH)_2$/NF	1 M KOH	10 mM HMF	230 mA cm^{-2}	FDCA (98%)	–	Achieving industrial-relevant current density in HMFOR. Reduction of Ni^{3+} to Ni^{2+} occurs during HMFOR	[92]
Ni_xB@NF	1 M KOH	10 mM HMF	1.45 V	FDCA (99%)	40 min at 1.45 V (vs RHE)	Operando electrochemistry with ATR-IR shows HMF preferentially oxidized through 5-hydroxymethyl-2 furancarboxylic acid, not 2,5-diformylfuran. Ni^{3+} is found as a necessary prerequisite for HMFOR.	[109]
NiMn UT-LDHs	1 M KOH	10 mM HMF	1.37 V	FDCA (99%)	3 h at 10 mA cm^{-2}	Establishing a relation between catalysts' deprotonation propensity and selectivity of FDCA using operando synchrotron diffraction and spectroscopic techniques. Ni^{3+} is present as HMFOR in the entire potential range.	[89]
Ni_3N@C	1 M KOH	10 mM HMF	1.45 V	FDCA (98%)	15 h at −10 mA cm^{-2} for HER‖ HMFOR	Probing reaction mechanism by surface-selective vibrational spectroscopy using sum frequency generation (SFG).	[110]
NiB_x–P_y	0.1 M KOH	HMF	1.464 V	FDCA (92.5%)	–	Effect of P-doping into nickel boride lattice for HMFOR.	[111]
Ni_2P-NPA/NF	1 M KOH	10 mM HMF	1.35 V, 1.44 V	FDCA (98%)	12 h at −10 mA cm^{-2} for HER‖ HMFOR	A facile and efficient strategy for simultaneous H_2 production and biomass upgradation.	[112]
Ni_3S_2/NF	1 M KOH	10 mM HMF	1.35 V, 1.46 V	FDCA (98%)	18 h at −10 mA cm^{-2} for HER‖ HMFOR	Upgrading five representative biomass substrates with decoupled H_2 generation.	[113]
NiO/Ni	0.1 M NaOH	0.1 M glucose	1.51–1.91 V	C2–C4	2.5 h at 1.61 V (vs RHE)	Investigating of effect of several reaction parameters on product selectivity.	[114]
$NiFeN_x$	1 M KOH	100 mM glucose	1.39 V	Glucaric acid (87%)	14 h with five consecutive cycles	The reaction proceeds via a guluronic acid pathway evidenced by in situ infrared spectroscopy. Ni^{3+} is reduced during the reaction.	[115]
Ni-Mo-N/CFC	1 M KOH	0.1 M glycerol	1.36 V_{cell}	Formate (95%)	12 h at 10 mA cm^{-2}	The high yield of the formate with good stability and mechanism was investigated by the isotope labeling experiment.	[116]
β-$Ni(OH)_2$	1 M KOH	50 mM urea	1.65–1.75 V	Nitrogen (100%)	20 h at 1.4 V (vs RHE)	Nitrogen formation involves intramolecular coupling of the N—N bond, accompanied by processes such as PCET, hydration, and rearrangement. Ni^{2+} is the active site during UOR in a high concentration of urea (0.5 M)	[91]
$NiWO_4$	1 M KOH	0.5 M urea	1.6 V	–	20 h at 20 mA cm^{-2}	Operando investigation of the dynamic of Ni valence by XAS. Ni^{3+} species are mostly present throughout the entire potential range of UOR	[90]

SA- Single atom; NF- Nickel foam; LDH- Layered double hydroxide; hp- hierarchically porous; C- carbon; CFC- carbon fiber cloth; SDS- sodium dodecyl sulfonate; MOF-Metal organic framework.

Table 2. Oxidation state transformation of Ni-containing catalysts and their correlated roles in the OOR.

(Pre)Catalyst	Catalyst	Organic reactant	Oxidation state transformation (or evolution)	Mechanistic role	Refs.
Metallic Ni	$Ni(OH)_2$/NiOOH	Alcohols and amines	Ni^{3+} to Ni^{2+}	Hydrogen atom using hydroxyl radical generated from NiOOH	[85]
Metallic Ni	$Ni(OH)_2$/NiOOH	Aldehyde	Ni^{3+} to Ni^{2+}	–	[123]
NiOOH	$Ni(OH)_2$/NiOOH	Amines	Ni^{3+} to Ni^{2+} and Ni^{4+} to Ni^{3+}/Ni^{2+}	Indirect oxidation (H atom transfer) and potential dependent oxidation (hydride transfer to Ni^{4+})	[55]
Plasma-derived Ni(oxy)hydroxide on NF	NiOOH	HMF and Alcohol	$Ni^{3/4+}$	Electrophilic active oxygen species	[6]
Ultrathin Ni(Fe,Mn) layered hydroxide	Ni(Fe,Mn)OOH	HMF	$Ni^{3/4+}$ to Ni^{2+}	Proton transfer from HMF to $Ni^{3+/4+}$	[89]
$NiWO_4$	NiOOH	Urea	Ni^{3} to Ni^{2+}	Proton transfer from HMF to Ni^{3+} (likely)	[90]
Ni-M$(OH)_2$(Fe,Co,Mn. Ga,Mo,Cr)	Ni(M)OOH		Ni^{3+} to Ni^{2+}	Proton transfer from HMF to Ni^{3+}	[92]
NiTx (T = P, S, Se).	NiOOH-TO_x (T = P, S, Se)	MeOH	Ni^{3+} evolves (and disappears with OOR)	Oxidation through active oxygen species	[93]
NiB_x/Ni heterostructure	NiOOH	MeOH	Ni^{3+} evolves (and disappears with OOR)	Oxidation through active oxygen species	[94]

also explored the doping of phosphorous (P) on the nickel borides (NiB_x) matrix and found that the optimum amount of P helped to increase the yield and faradic efficiency (FE) of HMFOR at a potential of 1.464 V (vs RHE) and concluded that P inclusion modified the surface electronic properties of nickel and nickel distribution on NiB_x-P_y catalyst.[111] A schematic reconstruction of a catalyst under an HMF environment is shown in Figure 9d. In another study, Du et al. further reinforced this chemical reduction of Ni^{3+} to Ni^{2+} in terms of HMFOR, from a reconstructed self-supported NiFeP/NF (pre)catalyst. Furthermore, they claimed Fe inclusion helped in the promotion effects and thus gave a better result toward HMFOR as compared to NiP/NF.[130] In contrast, our group has already reported the disadvantages of Fe for OOR. The intentional Fe inclusion on a plasma-treated NF, through CV, had been negatively influenced in several OORs as compared to OER. For a pure nickel catalyst, the RDS occurs after the initial adsorption and oxidation of OH^-/H_2O (i.e., *[O_e] formation), while for a nickel-iron catalyst, *[O_e] formation is the RDS step. Thus, Fe reduces the OER onset potential, which leads to a smaller potential window to selectively oxidize organic molecules (Figure 9e,f).[6] Another study from our group further emphasized the previous finding and showed iron free sample is more active for the HMFOR. However, in a potential window when the mass transport limitations are significant, both nickel and nickel-iron systems may exhibit similar conversion rates.[131]

Recently, Qu et al. fabricated phytic acid (PA) over NF via a hydrothermal route and applied it for the BAlOR, which resulted in an O*-dominated β-NiOOH active phase in the presence of BA and yielded a more competent catalyst than separately prepared NiOOH. This O*-dominated β-NiOOH had a higher capacity for α-C—H activation of alcohols. Such a tuning during synthesis changes the metal sites, thereby assisting in the biomass electrooxidation process.[132] Similarly, directly applying as-prepared samples for an electrooxidation reaction revealed a phase reconstruction after OOR. Schuhmann and co-workers prepared Ni_xB and following HMFOR, the catalyst underwent reconstruction resulting in a core–shell-like structure. In this structure, oxidized Ni species ($Ni(OH)_2$, NiO, and NiOOH) formed a shell while the synthesized Ni_xB remains in the core.[109] Moreover, they claimed that the formation of a higher metal oxidation state is the prerequisite for the electrochemical oxidation of alcohols and aldehydes, which was analogous to the findings of Nichols's group.[133] Similarly, Wang et al. also observed this phase change of their as-prepared Ni_3N@C electrode to NiOOH under HMFOR conditions.[110]

In one of the recent studies led by Bedford and co-workers, NiFe and NiMn LDH were synthesized along with defect-rich UT-LDHs of NiFe and NiMn. In this work, NiMn UT-LDHs displayed the highest FE of 99% from HMF to FDCA at the comparatively lower potential at 1.37 V (vs RHE). Additionally, when HMFOR performed in the OER potential window (@ 1.52 V vs RHE), an efficiency of 92.7% was obtained, in contrast only 49.5% FE was achieved by UT-NiFe LDH. The enhanced performance of UT-NiMn LDH is attributed to the greater avialablity of deprotonated sites due to its defects which, in turn, enhance the covalency along the M—O sites and weaken the O—H bonds during HMFOR. Further, Mn-OH sites delay the onset of OER during the HMFOR reaction, and more oxidized Mn—O sites during the HMFOR accepted protons and electrons from HMF and its intermediates by reducing metal sites from MnO_2 to MnOOH and finally to $Mn(OH)_2$.[89] Similarly, Feng et al. demonstrated that NiMn LDH outperforms NiFe LHD for MOR (Figure 9g). Although the mechanistic pathway of MOR on the NiMn/NiFe-LDHs are similar, however, in NiMn LDH the Ni^2/Ni^3 peaks ($^{ox}E/^{ox}E$ = 1.34/1.33 V (vs RHE) shift more cathodically compared to NiFe ($^{ox}E/^{ox}E$ = 1.44/1.42 V vs RHE). The easier oxidation of NiMn enhances the absorption of CH_3OH on the catalyst surface. Moreover, it is well known that Ni^2/Ni^3 oxidation of NiMn-LDH is quasi-irreversible, while NiFe-LDH is fully reversible. Consequently, the NiMn system proves to be a better choice for OORs

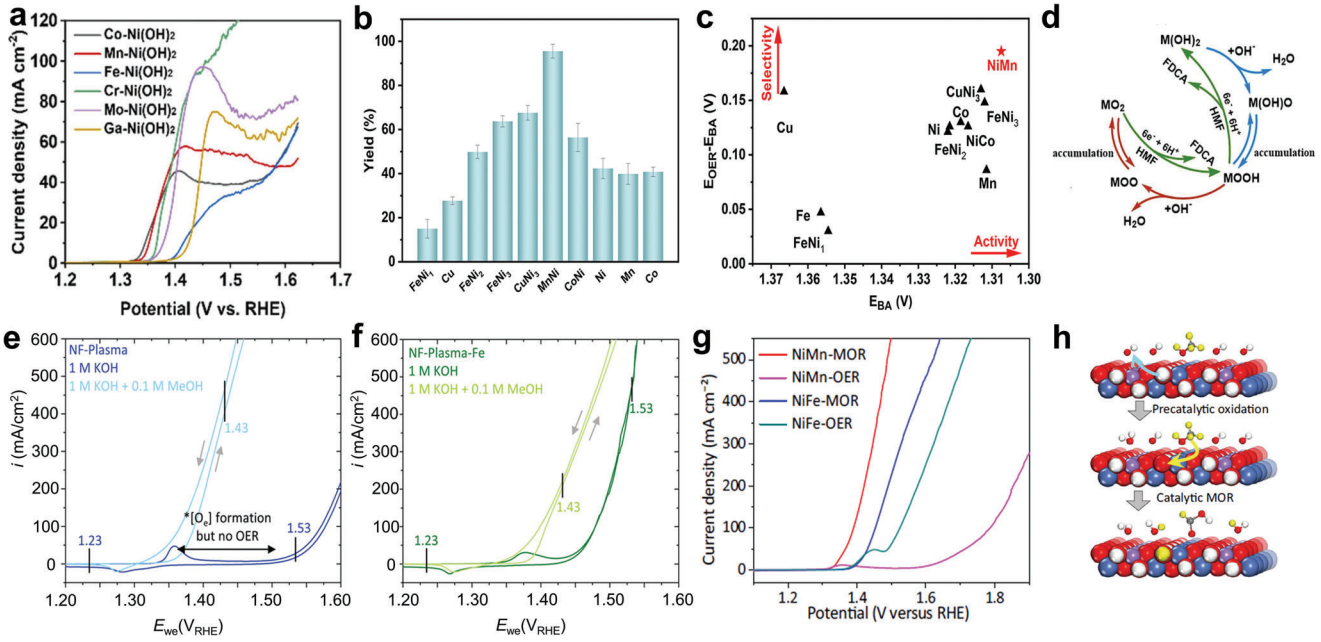

Figure 9. a) LSV curves of metal-doped (X-Ni(OH)$_2$) in 1 M KOH and 10 mM of HMF. Among these Cr-Ni(OH)$_2$ showed the best results toward HMFOR. Reproduced with permission.[92] Copyright 2023, Elsevier. b) Bar diagram of several TM-based catalysts, among them c) NiMn showing the best selectivity and activity toward BAmOR. Reproduced with permission.[75] Copyright 2022, American Chemical Society. d) Schematic of structural transformation and structure regeneration process during OER and HMFOR. Reproduced with permission.[89] Copyright 2023, Wiley-VCH. CVs (@ 5 mV s^{-1}, stirring) in 1 M KOH with and without MeOH of e) NF-Plasma and f) NF-Plasma-Fe. Reproduced with permission.[6] Copyright 2022, Wiley-VCH. g) LSV curves (*i*R-corrected) of NiMn and NiFe-LDHs were recorded in the presence of 3 M of CH_3OH in 1 M KOH. The results showed that NiMn was the better catalyst for MOR than NiFe. h) Reaction scheme for the overall MOR on NiMn/NiFe-LDHs. The blue and yellow arrows indicate the proton transfers during the precatalytic oxidation process. Reproduced with permission.[73] Copyright 2023, Nature.

than OER. For a better understanding, a general reaction scheme on the LDHs is shown in Figure 9h.[73] In line with the findings of our work, Feng's study also supports the notion that the NiFe system probably is not a good choice for MOR.[6,131]

Recently, several Ni-based chalcogenides and pnictides materials have been applied for several OOR reactions, due to their reconstruction benefit in the OOR regimes. Moreover, in the anodic potential, it is well known that chalcogenide or pnictide anion (X^{n-}) forms water-soluble oxyanions (XO_4^{2-} and XO_4^{3-}, according to Pourbaix diagrams) after leaching from the (pre)catalyst.[134] The oxyanions adsorb or intercalate on the catalyst surface, proving advantageous for OER by breaking the persistent *OH/*OOH scaling relations by stabilizing the reaction intermediate.[135] Hence, the presence of oxyanions opens up a new strategy to improve OER, as well as OOR reaction efficiency. In this regard, Liu et al. prepared chalcogen-doped Ni(OH)$_2$ that reconstructed to NiOOH with surface adsorbed chalcogenate species under reaction conditions. This reconstructed catalyst exhibited substantial advantages for amine electrooxidation, inducing the local electric field that impetuses the polar amines to easily pass through the inner Helmholtz plane to reach the catalyst surface more efficiently and boost amino C—N bond activation for dehydrogenation into nitrile C≡N bonds (**Figure 10**a,b). In situ Raman studies also showed the presence of SO_4^{2-} species in between 1.3 and 1.6 V (vs RHE) in the presence of propylamine substrate, while the HR-TEM consists of the <101> crystal plane of NiOOH. During the propylamine oxidation the Ni(OH)$_2$ structure evolved to NiOOH (Figure 10c,d).[70]

Wang et al. tuned the coordination environment of the Ni sites by introducing P, S, and Se, which reconstructed to NiOOH-TOx (TO_x = PO_x, SO_x, and SeO_x) and thus employed in the MOR. Among them, NiP_x-R (NiOOH-PO_x) showed the best results (Figure 10e). During the oxidation process pristine (pre)catalyst reconstructed to amorphous NiOOH coordinated with residual oxyanions. The HRTEM of NiP_x-R suggested a crystalline-amorphous interface and confirmed the formation of the Ni-hydroxide outer layer (Figure 10f). The presence of oxyanions tunes the coordination environments in the Ni sites of NiP_x-R and results in higher adsorption of OH* intermediates and methanol molecules. This facilitated MOR, which further validates why less activity was observed in the oxyanions-free NiOOH sample.[93]

In another study, Zhang et al. synthesized NiS_2 on carbon fiber cloth (NiS_2/CFC) by a facile vapor-phase hydrothermal (VPH) method and subsequently applied it to a series of alcohols (2-propanol, 2-butanol, 2-pentanol, and cyclohexanol) oxidation reaction. They conclude that oxidized Ni species are responsible for the oxidation of alcohols to ketones.[101] At the same time, Sun et al. also prepared hierarchically porous Ni_3S_2 on NF (Ni_3S_2/NF) and studied various OORs. After OORs, they also observed the formation of oxidized Ni (nickel oxides/hydroxides and (oxy)hydroxides) and S species.[113] A similar observation was made by Sun and co-workers when preparing 3D Ni_2P nanoparticle arrays on NF (Ni_2PNPA/NF), which was then directly applied for the HMFOR displaying, the role of oxidized Ni species in the oxidation of HMF.[112]

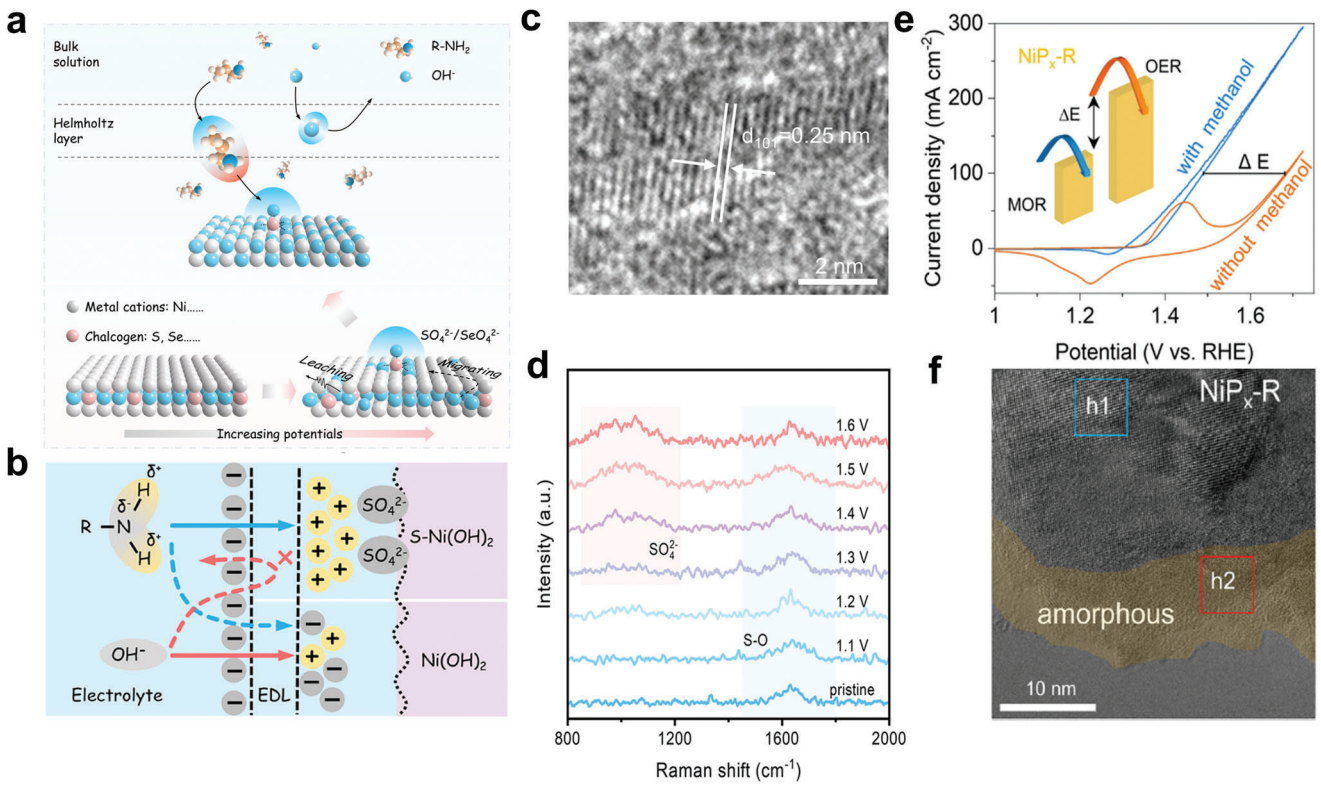

Figure 10. a) Schematic representation of in situ chalcogen leaching from (pre)catalyst for tuning the reactant/surface interface toward amine electrooxidation. b) Plausible mechanism in the reactant interface governed by the adsorbed chalcogenate species. The blue solid arrow shows how the presence of SO_4^{2-} attracts the amine by increasing the positive charge near the surface of the catalyst. c) HR-TEM image for S-Ni(OH)$_2$ catalysts after POR exhibiting (101) (d = 0.25 nm) plane of NiOOH. This provided an idea about the transformation of Ni(OH)$_2$ to NiOOH during POR. d) In situ Raman spectra of S-Ni(OH)$_2$ in the presence of 1 M KOH with 100 mmol of propylamine. The presence of SO_4^{2-} was detected within the potential range of 1.3 to 1.6 V. Panels (a–d) were reproduced with permission.[70] Copyright 2022, American Chemical Society. e) Polarization curves of NiP$_x$-R in 1 M KOH solution with and without 0.5 M methanol. f) HR-TEM image of NiP$_x$-R after MOR demonstrating a surface reconstruction to a crystalline-amorphous interface. Panels (e) and (f) were reproduced with permission.[93] Copyright 2022, Nature.

Deliberate or adventitious intercalation is beneficial in improving the catalytic activity of several OORs. In an interesting study, Duan and colleagues synthesized sodium dodecyl sulfonate (SDS) intercalated Ni(OH)$_2$ (**Figure 11**a,b). This intentional intercalation of SDS between two layers of Ni(OH)$_2$ resulted in a remarkable 3.6-fold improvement in activity compared to pristine Ni(OH)$_2$. Simultaneously, it enhanced the solubility of cyclohexanone in the aqueous medium (0.5 M KOH) to selectively produce adipic acid, a key monomer in Nylon-66. The incorporation of negatively charged dodecyl sulfate anions in the interstitial 2D layers of Ni(OH)$_2$ fine-tuned the local environments of the active sites, proving beneficial in improving the activity.[104] Along this line, recently, we also reported the in situ generated carbonate intercalated γ-NiOOH as a suitable catalyst for the selective oxidation of HMF, BAl, and BAm to their corresponding value-added product.[103] This intercalation strategy is also useful for UOR, as disclosed by Qiao and co-workers in their studies. During activation, pristine NiS_2 was reconstructed to a crystalline NiS_2 core and a 2–5 nm thick amorphous NiOOH shell with oxidized sulfur species. This study further disclosed that oxyanion tailored the Ni sites, enhancing UOR by suppressing water oxidation.[136] Moreover, strategically synthesized core–shell-like structures have proven to improve the active site density and formed an electronically conductive framework, which was explored by Wang and co-workers in their studies. They applied Ni-foam-supported Ni@Ni_2P core–shell nanotube for the hydrazine electrooxidation reaction.[137]

All the above-mentioned examples highlight the phase changes occurring during OOR and simultaneously oxidizing organic molecules via a potential dependent or "indirect reaction" pathway, an idea initially proposed by Fleischmann et al. for amines and alcohols in the early 1970s.[83,85] Nevertheless, the in situ phase changes of NiOOH decoupled with various chemical and electronic factors, play an important role in dictating the selectivity and reactivity of those reactions. In this regard, Yan et al. synthesized β-NiOOH and γ-NiOOH phases and studied their oxidative properties. They observed that β-NiOOH was highly reactive (>95% conversion) and selective (>95% selectivity) for the dehydrogenation of alcohols, while γ-NiOOH led to the formation of byproducts. Furthermore, overoxidation from β-NiOOH to γ-NiOOH negatively impacted the overall selectivity in the mass transport limited regime (Figure 11c). A flow cell setup could be a suitable alternative to tackle this problem. Therefore, their study also explored the influence of solvents on the reaction rate, however, less influence on the selectivity of the reactions was observed.[122] As we discussed earlier, the existence

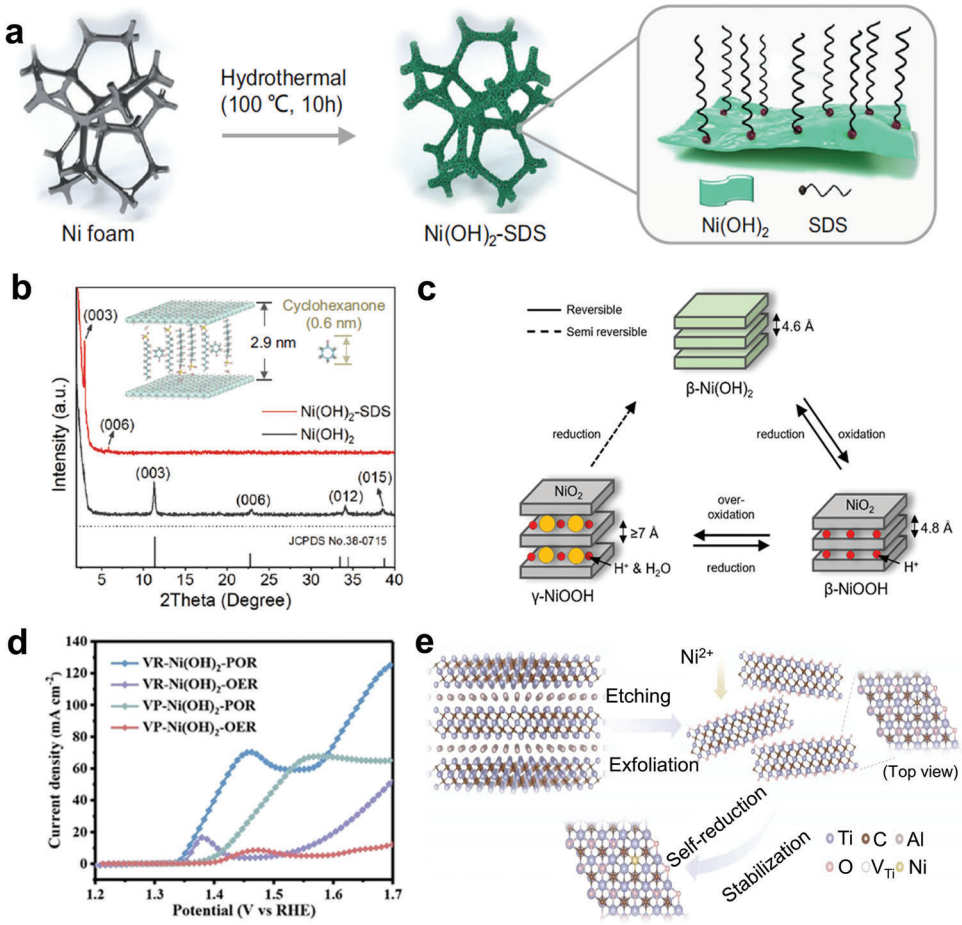

Figure 11. a) Schematic demonstration of a step-wise fabrication process of $Ni(OH)_2$-SDS grown on Ni foam. SDS was used as an intercalating agent during the synthesis, which helped to increase the interlayer spacing of the $Ni(OH)_2$ and b) XRD spectra comparing the patterns of $Ni(OH)_2$-SDS and pristine $Ni(OH)_2$ samples. Panels (a) and (b) were reproduced with permission.[104] Copyright 2022, Nature. c) Illustration showing the transformation of NiOOH from one phase to another under operating conditions.[122] Copyright 2023, American Chemical Society. d) Normalized LSV curves with and without 10 mmol of propylamine in 1 M KOH. Vacancy rich (VR)-$Ni(OH)_2$ phase demonstrated better results in both OER and POR. Reproduced with permission.[139] Copyright 2020, Wiley-VCH. e) Schematic of Ni SACs/$Ti_3C_2T_x$ synthesis process. The etching and exfoliation resulted in vacancy formation on the surface of the 2D MXene phase and has proven to be a reactive site to bind hydrazine molecules. Reproduced with permission.[106] Copyright 2023, Wiley-VCH.

of Fe in the (pre)catalyst was not a suitable choice for OOR reactions in an alkaline medium. Regrettably, the presence of the nominal amount of Fe in the electrolyte (as an impurity) cannot be ruled out, which participates during the catalyst reconstruction and its affinity toward Ni-based material was already well known in OER.[138] In this line, Hahn and co-workers observed the influence of metal (Fe) impurities (originating from unpurified electrolytes), during the BAlOR and deduced a strong correlation between Ni-redox onset potential. The presence of Fe (≈7–18%) in the reconstructed Ni-Fe electrodes also tuned the local structure by creating O-vacancy at the bridge sites of the Fe–NiOOH lattice.[102] Such a vacancy-rich system was also beneficial for amine oxidation, aligning with the findings of Zhai et al., who reported the benefits of vacancy-rich $Ni(OH)_2$ over vacancy-poor $Ni(OH)_2$. They modified the Ni-MOF precursor directly under electrochemical conditions to obtain the vacancy-rich $Ni(OH)_2$ phase, which induces local electropositive and facilitates N atoms (consisting of a lone pair of electrons) to bind in the reaction sites. This subsequently attacks N(sp^3)-H, and accelerates amino C—N bond activation for dehydrogenation reactions (Figure 11d).[139] One of the recently developed concepts of single-atom catalysts (SACs) has also gained noticeable attention from the scientific community.[140] Utilizing a maximum number of metal sites and their unsaturated coordination state provides a versatile platform for several reactions including CO oxidation[141] and ammonia synthesis.[142] To explore this avenue, Yuan and co-workers synthesized Ni single atoms on a 2D MXene surface, which leads to a vacancy-rich electrocatalyst for hydrazine-oxidation reaction (Figure 11e).[106]

The pivotal step in OOR (with —OH, —NH_2, —CHO functional groups) is the abstraction of a proton (or transfer of a hydrogen atom, or a hydride ion) from the organic reactant. An alternative to this step remains elusive, and it is likely independent of the structure of the starting reagent, encompassing various functional groups, cyclic structures, aromatic groups, etc. Nonetheless, the reaction rate, selectivity, and formation of

by-products are observed to be contingent upon the compound's structure.[45,68,85,105,143] To date, understanding the interconnection between the active phase (of the anode material) and the molecular structure, geometry, or stereochemical orientation of functional groups in the organic reactant is merely investigated. It is crucial to emphasize that the nature of the catalytic phase alone does not solely determine conversion efficiency and product selectivity; several other factors such as the pKa of the reactant, local pH, electronic factors, orientation of organic molecules (and related intermediates) during adsorption on the catalyst surface, mass transportation,[2,70,102] may exert greater influence.[131] Predicting the significance of a parameter is fraught with uncertainty. Nevertheless, with a Ni-containing anode, the potential value commonly employed to oxidize organics, such as alcohols, amines, and aldehydes, is sufficient to oxidize lower valent Ni species (e.g., Ni^{2+}) into higher valent species ($Ni^{3+/4+}$). Thus, even if Ni^{2+} is produced during proton abstraction, it rapidly regenerates $Ni^{3+/4+}$ due to the applied potential. This dynamic process, unique to each organic reactant, results in Ni-oxo species with varying hydration, morphology, defects, short-range order, etc. Despite available literature, conclusively determining such an active phase structure correlated with the organic reactant is nearly impossible. While in situ measurements offer insights into determining such an active structure, complexities related to interpreting phase change dynamics and solubility issues with large organic molecules render the experiments exceedingly challenging to manage.

In summary, the exploration of Ni's multifaceted role in electrochemical OOR reveals a nuanced interplay of various factors as discussed before. Several parameters, such as doping, leaching, exfoliation, intentional or unintentional intercalation, impurity management, vacancy control, and the introduction of secondary metals or metalloids, have demonstrably augmented catalytic activity across the diverse OOR process. These strategies have emerged as indispensable tools for not only elevating the reaction rates but also fine-tuning the selectivity toward desired valuable products. As researchers continue to unravel the intricate intricacies of Ni's involvement in electrochemical transformations, this comprehensive understanding opens avenues for the design and optimization of advanced catalysts in organic synthesis.

5. Conclusions and Future Perspectives

This comprehensive review encapsulates recent advancements in the field of OOR, emerging as a suitable alternative for energy-demanding OER. Notably, nickel constitutes as a promising central metal for anode catalysts in these reactions. This review delves into the significant developments in electrochemical OOR that highlight nickel's role as a catalyst in enhancing oxidation efficiency and product selectivity. So far, it has been realized that the anodically wired hydrated nickel oxide is one of the promising active catalysts, which reversibly switches between lower to higher oxidation states and oxidizes organic molecules. Apart from this, electrode design, catalyst morphology, doping of foreign elements, leaching or adsorbing of chalcogens (oxyanions), the introduction of the intercalating species, precise reaction conditions, electrolyte pH, along with the type of cell, and membrane (in the case of the divided cell) determine the overall cell activity and efficiency of OORs but are mostly underrepresented. **Figure 12** illustrates the transformative advancements in electrochemical OOR research, highlighting a future trajectory advanced by cutting-edge methodologies. The diagram outlines the progression through operando studies, enabling real-time insights into the electrocatalytic processes. Further, the exploration of novel coupling reactions is depicted, demonstrating a forward-looking approach to catalytic efficiency for specific reactions. The integration of flow cells for high-rate applications and industrial-scale current densities signifies a pivotal stride toward practical implementation. Additionally, the figure emphasizes the meticulous investigation of electrode-electrolyte interfaces and underlines the optimized utilization of density functional theory (DFT) for unparalleled breakthroughs, elucidating a comprehensive framework for reforming electrochemical OOR in the near future. Therefore, significant research efforts are required to propel this technology toward widespread commercialization, and we highlighted the frontline aspects as follows:

1) Both OER and OOR are thermodynamically uphill processes. In general, OOR requires even more overpotential as compared to OER when both involve the same number of electron and protons transfer. Essentially, minimizing overpotential and thereby increasing the reaction rate largely depends on the catalyst engineering aspect, which is predominantly contributed by the anode materials and their catalytic hotspots. In this view, analytical techniques under operando conditions and DFT calculation also need significant care to determine such catalytic hotspots. It is important to note that acquiring meaningful results from DFT calculations is often very challenging as the thermodynamics are often considered without transition states, complex heterogeneity in the phases, and multiple chemical environments around catalytic hotspots, thus, resulting in DFT calculation not being straightforward. All of these parameters must be critically assessed and compared with experimental data and reported literature.[144]
2) Most of the electrochemical oxidation processes are reported only based on alcohols, amines, urea, ammonia, and biomass (HMF) hydroxylation or dehydrogenation. Moreover, the reaction conditions,[145] chemical additives, and suitable organic substrate are also little known to get oxidative coupling reactions. The limitation in substrate scope is partly attributed to the use of an aqueous (particularly alkaline) reaction medium, restricting solubility for a broader range of organic compounds. Therefore, a wide range of aqueous organic solvent mixtures could expand the feasibility of the substrate scope in addition to the other operational parameters.
3) Unlike OER, OOR is diffusion-controlled, necessitating careful attention to identify potential oxidation regions where mass transportation is a limiting factor. In this regard, it is important to know the redox features of the catalysts.[131] Moreover, to overcome this, significant research should be dedicated to constructing suitable electrode assemblies including membrane engineering and flow cell setups.
4) The introduction of organic compounds in solutions alters the microenvironment, diverging from typical water systems. This change influences electron transfer processes, redox reactions,[103] and electrochemical potential gradients, while also impacting pH levels within the system. Such a diverse

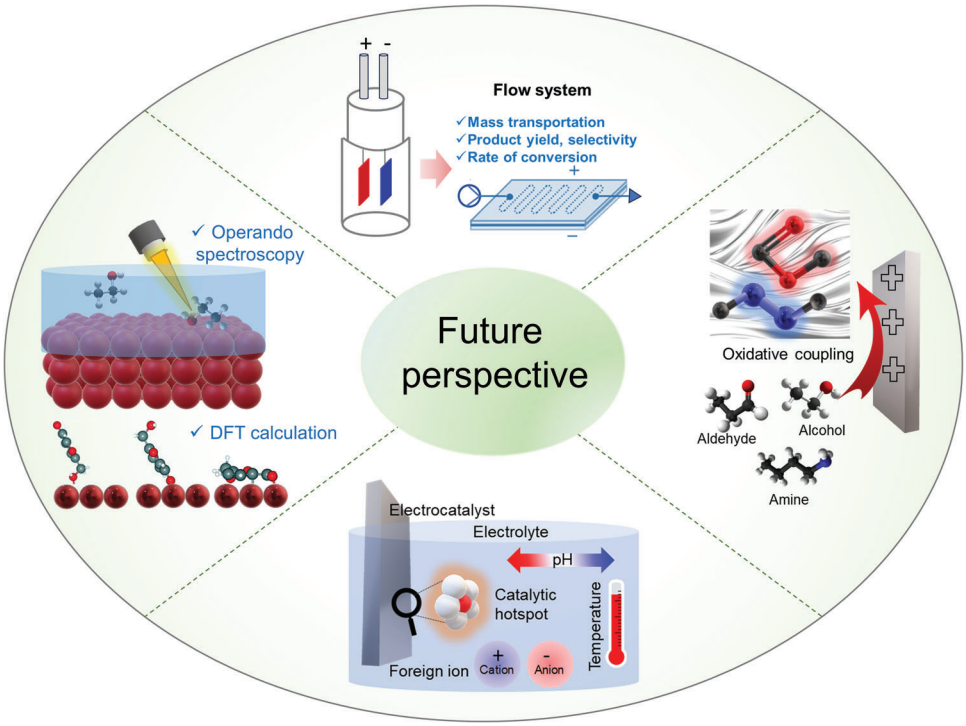

Figure 12. Revolutionizing electrochemical OOR in future direction: Advancing through operando studies, exploration of new coupling reactions, use of flow cells for high-rate and industrial relevant current densities, meticulous electrode-electrolyte interface investigation, and optimized DFT utilization for unparalleled breakthroughs.

microenvironment plays a significant role in Raman spectroscopy measurements as well, especially considering its sensitivity to surface properties.[38,146] This technique has been invaluable in identifying active species during reactions, particularly in OORs. In contrast to reactions, like the OER, OORs pose unique challenges related to the movement and mixing of substances at the reaction site. Factors, such as the local concentration of reactants and their interaction with the surface, greatly influence which species are involved in the reaction. Additionally, the solubility of reactants in water and the rate at which reaction products detach from the surface impact the observations made during Raman spectroscopy.[70] Active species formed during OORs typically exhibit more defects compared to traditional metal-based species. This is due to the constant switching between high and low oxidation states of metal centers, leading to imperfections in the structure of the active species.[92] That cannot truly be revealed by Raman Spectroscopy. Moreover, the interface between the electrode and the electrolyte, where the reaction occurs, significantly affects the behavior of electrochemical sites.[147] This influence can alter the shape and position of the observed Raman peaks.[148] To accurately interpret Raman spectra in OORs, standardization of the data is essential. This involves establishing a consistent background against which we can compare observations in the presence and absence of reactants. Additionally, using reference samples containing the same active species aids in confidently identifying true active species in the reaction.

5) In parallel, it is also important to know to what extent organic oxidation is truly electrochemical. Certain organic molecules, such as aldehydes, undergo oxidation much earlier than the redox event of most TM catalysts. In this situation, the use of a catalyst is questionable. Therefore, there is a pressing need to explore suitable catalysts and establish their correlation with the working potential region to obtain the desired selectivity in organic product formation.
6) Various studies demonstrate paired electrolysis using a divided cell, while the effectiveness of this technique in reducing product crossover and enhancing chemoselectivity is not unequivocal. Moreover, the influence of proton and electron conductivity in the divided cell, and the efficiency or selectivity losses upon product contact with the cathode, remains largely unexplored. A recent advancement to implement industrial-relevant conditions (≥6 M KOH, ≥65 °C) is often used to test the OER activity for the mass production of H_2 and decrease the overall cell potential (as a function of temperature) of overall water electrolysis, which has not been explored extensively for OORs.[145] Knowing that the yield and selectivity of the OORs are largely dependent on temperature and solvent conditions, it can suitably be coupled with industrial-relevant OER conditions attributing to great industrial importance.
7) Product purification from the electrolyte solution must be more simplified and should run under low-cost operating techniques. Importantly, the techno-economic factor must be analyzed of the OOR oxidized products.[4] In this regard, the cost of reactants, the selling price of the product, their availability, carbon footprints, hydrogen production rate, and

demand for the oxidized product, all must be considered thoroughly.

Our collective effort aims to delineate specific aspects that have promising prospects for future research in the OOR field, with nickel being the favorable choice of metal to attend to these objectives.

Acknowledgements

S.G., D.B., and I.M. contributed equally to this work. The authors greatly acknowledge support from the German Federal Ministry of Education and Research (BMBF) in the framework of the project Catlab (03EW0015A/B) and BMBF project "PrometH_2eus," 03HY105C. The authors would like to thank Prof. Dr. Matthias Driess for the scientific infrastructure. R.V.J. thanks the European Union under the REFRESH – Research Excellence for Region Sustainability and High-tech Industries project number CZ.10.03.01/00/22_003/0000048 via the Operational Programme Just Transition for general and financial support. I. M thanks SERB Ramanujan fellowship.

Open access funding enabled and organized by Projekt DEAL.

Conflict of Interest

The authors declare no conflict of interest.

Keywords

in situ studies, Ni-based (pre)catalyst, organic oxidation reactions, paired electrolysis, reconstruction, redox-active site, valorization of biomass-based feedstocks

Received: February 10, 2024
Revised: March 18, 2024
Published online: April 8, 2024

[1] P. Achakulwisut, P. Erickson, C. Guivarch, R. Schaeffer, E. Brutschin, S. Pye, *Nat. Commun.* **2023**, *14*, 5425.
[2] Y. Kwon, S. C. S. Lai, P. Rodriguez, M. T. M. Koper, *J. Am. Chem. Soc.* **2011**, *133*, 6914.
[3] F. Xiao, Q. Wang, G.-L. Xu, X. Qin, I. Hwang, C.-J. Sun, M. Liu, W. Hua, H.-w. Wu, S. Zhu, J.-C. Li, J.-G. Wang, Y. Zhu, D. Wu, Z. Wei, M. Gu, K. Amine, M. Shao, *Nat. Catal.* **2022**, *5*, 503.
[4] T. Kahlstorf, J. N. Hausmann, T. Sontheimer, P. W. Menezes, *Global Challenges* **2023**, *7*, 2200242.
[5] Q. Liang, G. Brocks, A. Bieberle-Hütter, *JPhys Energy* **2021**, *3*, 026001.
[6] J. N. Hausmann, P. V. Menezes, G. Vijaykumar, K. Laun, T. Diemant, I. Zebger, T. Jacob, M. Driess, P. W. Menezes, *Adv. Energy Mater.* **2022**, *12*, 2202098.
[7] Z. Chen, H. Yang, S. Mebs, H. Dau, M. Driess, Z. Wang, Z. Kang, P. W. Menezes, *Adv. Mater.* **2023**, *35*, 2208337.
[8] S. Ghosh, A. Mondal, G. Tudu, S. Ghosh, H. V. S. R. M. Koppisetti, H. R. Inta, D. Saha, V. Mahalingam, *ACS Sustainable Chem. Eng.* **2022**, *10*, 7265.
[9] S. Mondal, M. Riyaz, D. Bagchi, N. Dutta, A. K. Singh, C. P. Vinod, S. C. Peter, *ACS Nano* **2023**, *17*, 23169.
[10] R. Mehmood, W. Fan, X. Hu, J. Li, P. Liu, Y. Zhang, Z. Zhou, J. Wang, M. Liu, F. Zhang, *J. Am. Chem. Soc.* **2023**, *145*, 12206.
[11] L. Reith, J. N. Hausmann, S. Mebs, I. Mondal, H. Dau, M. Driess, P. W. Menezes, *Adv. Energy Mater.* **2023**, *13*, 2203886.
[12] F. Bao, E. Kemppainen, I. Dorbandt, F. Xi, R. Bors, N. Maticiuc, R. Wenisch, R. Bagacki, C. Schary, U. Michalczik, P. Bogdanoff, I. Lauermann, R. van de Krol, R. Schlatmann, S. Calnan, *ACS Catal.* **2021**, *11*, 10537.
[13] R. Farhat, J. Dhainy, L. I. Halaoui, *ACS Catal.* **2020**, *10*, 20.
[14] S. Zou, M. S. Burke, M. G. Kast, J. Fan, N. Danilovic, S. W. Boettcher, *Chem. Mater.* **2015**, *27*, 8011.
[15] G. Chen, X. Li, X. Feng, *Angew. Chem., Int. Ed.* **2022**, *61*, 202209014.
[16] F. W. S. Lucas, R. G. Grim, S. A. Tacey, C. A. Downes, J. Hasse, A. M. Roman, C. A. Farberow, J. A. Schaidle, A. Holewinski, *ACS Energy Lett.* **2021**, *6*, 1205.
[17] A. G. Oshchepkov, G. Braesch, A. Bonnefont, E. R. Savinova, M. Chatenet, *ACS Catal.* **2020**, *10*, 7043.
[18] P. W. Menezes, C. Walter, B. Chakraborty, J. N. Hausmann, I. Zaharieva, A. Frick, E. von Hauff, H. Dau, M. Driess, *Adv. Mater.* **2021**, *33*, 2004098.
[19] J. Na, B. Seo, J. Kim, C. W. Lee, H. Lee, Y. J. Hwang, B. K. Min, D. K. Lee, H.-S. Oh, U. Lee, *Nat. Commun.* **2019**, *10*, 5193.
[20] D. Bagchi, S. Roy, S. C. Sarma, S. C. Peter, *Adv. Funct. Mater.* **2022**, *32*, 2209023.
[21] D. Bagchi, J. Raj, A. K. Singh, A. Cherevotan, S. Roy, K. S. Manoj, C. P. Vinod, S. C. Peter, *Adv. Mater.* **2022**, *34*, 2109426.
[22] W. F. Hoelderich, F. Kollmer, *Pure Appl. Chem.* **2000**, *72*, 1273.
[23] S. Caron, R. W. Dugger, S. G. Ruggeri, J. A. Ragan, D. H. B. Ripin, *Chem. Rev.* **2006**, *106*, 2943.
[24] K.-N. T. Tseng, A. M. Rizzi, N. K. Szymczak, *J. Am. Chem. Soc.* **2013**, *135*, 16352.
[25] D. Jeong, H. Kim, J. Cho, *J. Am. Chem. Soc.* **2023**, *145*, 888.
[26] W.-Y. Tan, Y. Lu, J.-F. Zhao, W. Chen, H. Zhang, *Org. Lett.* **2021**, *23*, 6648.
[27] L. F. T. Novaes, J. Liu, Y. Shen, L. Lu, J. M. Meinhardt, S. Lin, *Chem. Soc. Rev.* **2021**, *50*, 7941.
[28] R. Holze, *J. Solid State Electrochem.* **2020**, *24*, 1709.
[29] B. A. Frontana-Uribe, R. D. Little, J. G. Ibanez, A. Palma, R. Vasquez-Medrano, *Green Chem.* **2010**, *12*, 2099.
[30] C. Gütz, B. Klöckner, S. R. Waldvogel, *Org. Process Res. Dev.* **2016**, *20*, 26.
[31] H. Yang, G. Vijaykumar, Z. Chen, J. N. Hausmann, I. Mondal, S. Ghosh, V. C. J. Nicolaus, K. Laun, I. Zebger, M. Driess, P. W. Menezes, *Adv. Funct. Mater.* **2023**, *33*, 2303702.
[32] M. Rafiee, K. C. Miles, S. S. Stahl, *J. Am. Chem. Soc.* **2015**, *137*, 14751.
[33] M. Rafiee, Z. M. Konz, M. D. Graaf, H. F. Koolman, S. S. Stahl, *ACS Catal.* **2018**, *8*, 6738.
[34] M. F. Semmelhack, C. R. Schmid, *J. Am. Chem. Soc.* **1983**, *105*, 6732.
[35] F. Wang, S. S. Stahl, *Acc. Chem. Res.* **2020**, *53*, 561.
[36] P. Niu, X. Liu, Z. Shen, M. Li, *Molecules* **2019**, *24*, 100.
[37] A. Das, S. S. Stahl, *Angew. Chem., Int. Ed.* **2017**, *56*, 8892.
[38] I. Mondal, P. V. Menezes, K. Laun, T. Diemant, M. Al-Shakran, I. Zebger, T. Jacob, M. Driess, P. W. Menezes, *ACS Nano* **2023**, *17*, 14043.
[39] S. Roy, D. Bagchi, L. Dheer, S. C. Sarma, V. Rajaji, C. Narayana, U. V. Waghmare, S. C. Peter, *Appl. Catal., B* **2021**, *298*, 120560.
[40] S. Chakraborty, S. Marappa, S. Agarwal, D. Bagchi, A. Rao, C. P. Vinod, S. C. Peter, A. Singh, M. Eswaramoorthy, *ACS Appl. Mater. Interfaces* **2022**, *14*, 31951.
[41] A. K. Singh, D. Bagchi, S. Sarkar, S. C. Sarma, D. Mumbaraddi, S. D. Ramarao, S. C. Peter, *Chem. Mater.* **2022**, *34*, 8999.
[42] A. R. Rajamani, P. C. Ashly, L. Dheer, S. C. Sarma, S. Sarkar, D. Bagchi, U. V. Waghmare, S. C. Peter, *ACS Appl. Energy Mater.* **2019**, *2*, 7132.
[43] B. Dasgupta, J. N. Hausmann, R. Beltrán-Suito, S. Kalra, K. Laun, I. Zebger, M. Driess, P. W. Menezes, *Small* **2023**, *19*, 2301258.

[44] S. Ghosh, B. Dasgupta, C. Walter, P. W. Menezes, M. Driess, *Small Sci.* **2023**, *3*, 2200115.
[45] I. Mondal, J. N. Hausmann, G. Vijaykumar, S. Mebs, H. Dau, M. Driess, P. W. Menezes, *Adv. Energy Mater.* **2022**, *12*, 2200269.
[46] J. van Drunen, T. W. Napporn, B. Kokoh, G. Jerkiewicz, *J. Electroanal. Chem.* **2014**, *716*, 120.
[47] H. Yang, P. V. Menezes, G. Dai, G. Vijaykumar, Z. Chen, M. Al-Shakran, T. Jacob, M. Driess, P. W. Menezes, *Appl. Catal.* **2023**, *324*, 122249.
[48] X. Liu, X. He, Z. Fang, S. Gong, D. Xiong, W. Chen, J. Wang, Z. Chen, *Chem. Mater.* **2024**, *36*, 968.
[49] D. S. P. Cardoso, B. Šljukić, D. M. F. Santos, C. A. C. Sequeira, *Org. Process Res. Dev.* **2017**, *21*, 1213.
[50] L. Xu, Z. Huang, M. Yang, J. Wu, W. Chen, Y. Wu, Y. Pan, Y. Lu, Y. Zou, S. Wang, *Angew. Chem., Int. Ed.* **2022**, *61*, 202210123.
[51] T. Noël, Y. Cao, G. Laudadio, *Acc. Chem. Res.* **2019**, *52*, 2858.
[52] C. M. Crombie, R. J. Lewis, R. L. Taylor, D. J. Morgan, T. E. Davies, A. Folli, D. M. Murphy, J. K. Edwards, J. Qi, H. Jiang, C. J. Kiely, X. Liu, M. S. Skjøth-Rasmussen, G. J. Hutchings, *ACS Catal.* **2021**, *11*, 2701.
[53] E. Fabbri, T. J. Schmidt, *ACS Catal.* **2018**, *8*, 9765.
[54] J. N. Hausmann, R. Beltrán-Suito, S. Mebs, V. Hlukhyy, T. F. Fässler, H. Dau, M. Driess, P. W. Menezes, *Adv. Mater.* **2021**, *33*, 2008823.
[55] M. T. Bender, K.-S. Choi, *JACS Au* **2022**, *2*, 1169.
[56] G. Fu, X. Kang, Y. Zhang, Y. Guo, Z. Li, J. Liu, L. Wang, J. Zhang, X.-Z. Fu, J.-L. Luo, *Nat. Commun.* **2023**, *14*, 8395.
[57] Y. Yang, T. Mu, *Green Chem.* **2021**, *23*, 4228.
[58] W.-J. Liu, L. Dang, Z. Xu, H.-Q. Yu, S. Jin, G. W. Huber, *ACS Catal.* **2018**, *8*, 5533.
[59] Z. Lin, X. Chen, L. Lu, X. Yao, C. Zhai, H. Tao, *Nanotechnol. Rev.* **2023**, *12*, 20220518.
[60] H. Ait Rass, N. Essayem, M. Besson, *ChemSusChem* **2015**, *8*, 1206.
[61] W. Ge, L. Lin, S.-Q. Wang, Y. Wang, X. Ma, Q. An, L. Zhao, *J. Mater. Chem. A* **2023**, *11*, 15100.
[62] E. Pérez-Gallent, C. Sánchez-Martínez, L. F. G. Geers, S. Turk, R. Latsuzbaia, E. L. V. Goetheer, *Ind. Eng. Chem. Res.* **2020**, *59*, 5648.
[63] I. García-López, L. F. Arenas, T. Turek, V. I. Águeda, A. Garrido-Escudero, *React. Chem. Eng.* **2023**, *8*, 1776.
[64] Z. Kou, X. Li, L. Zhang, W. Zang, X. Gao, J. Wang, *Small Sci.* **2021**, *1*, 2100011.
[65] F. Lapointe, M. Wolf, R. K. Campen, Y. Tong, *J. Am. Chem. Soc.* **2020**, *142*, 18619.
[66] S. Xie, D. Li, H. Huang, F. Zhang, Y. Chen, *J. Am. Chem. Soc.* **2019**, *141*, 16237.
[67] M. Favaro, B. Jeong, P. N. Ross, J. Yano, Z. Hussain, Z. Liu, E. J. Crumlin, *Nat. Commun.* **2016**, *7*, 12695.
[68] Y. Hao, J. Li, X. Cao, L. Meng, J. Wu, X. Yang, Y. Li, Z. Liu, M. Gong, *ACS Catal.* **2023**, *13*, 2916.
[69] B. You, X. Liu, X. Liu, Y. Sun, *ACS Catal.* **2017**, *7*, 4564.
[70] Q. Wen, Y. Lin, Y. Yang, R. Gao, N. Ouyang, D. Ding, Y. Liu, T. Zhai, *ACS Nano* **2022**, *16*, 9572.
[71] Y.-C. Zhang, C. Han, J. Gao, L. Pan, J. Wu, X.-D. Zhu, J.-J. Zou, *ACS Catal.* **2021**, *11*, 12485.
[72] M. T. Bender, Y. C. Lam, S. Hammes-Schiffer, K.-S. Choi, *J. Am. Chem. Soc.* **2020**, *142*, 21538.
[73] B. Zhu, B. Dong, F. Wang, Q. Yang, Y. He, C. Zhang, P. Jin, L. Feng, *Nat. Commun.* **2023**, *14*, 1686.
[74] S.-K. Geng, Y. Zheng, S.-Q. Li, H. Su, X. Zhao, J. Hu, H.-B. Shu, M. Jaroniec, P. Chen, Q.-H. Liu, S.-Z. Qiao, *Nat. Energy* **2021**, *6*, 904.
[75] Y. Sun, H. Shin, F. Wang, B. Tian, C.-W. Chiang, S. Liu, X. Li, Y. Wang, L. Tang, W. A. Goddard III, M. Ding, *J. Am. Chem. Soc.* **2022**, *144*, 15185.
[76] S. L. Medway, C. A. Lucas, A. Kowal, R. J. Nichols, D. Johnson, *J. Electroanal. Chem.* **2006**, *587*, 172.
[77] W. Visscher, E. Barendrecht, *Surf. Sci.* **1983**, *135*, 436.
[78] D. S. Hall, C. Bock, B. R. MacDougall, *J. Electrochem. Soc.* **2013**, *160*, F235.
[79] P. A. Alaba, C. S. Lee, F. Abnisa, M. K. Aroua, P. Cognet, Y. Pérès, W. M. A. Wan Daud, *Rev. Chem. Eng.* **2021**, *37*, 779.
[80] M. Alsabet, M. Grdeń, G. J. E. Jerkiewicz, *Electrocatalysis* **2011**, *2*, 317.
[81] B. J. Trześniewski, O. Diaz-Morales, D. A. Vermaas, A. Longo, W. Bras, M. T. M. Koper, W. A. Smith, *J. Am. Chem. Soc.* **2015**, *137*, 15112.
[82] Y. L. Lo, B. J. Hwang, *Langmuir* **1998**, *14*, 944.
[83] M. Fleischmann, K. Korinek, D. Pletcher, *J. Chem. Soc., Perkin Trans. 2* **1972**, https://doi.org/10.1039/P29720001396.
[84] M. T. Bender, R. E. Warburton, S. Hammes-Schiffer, K.-S. Choi, *ACS Catal.* **2021**, *11*, 15110.
[85] M. Fleischmann, K. Korinek, D. Pletcher, *J. Electroanal. Chem. Interfacial Electrochem.* **1971**, *31*, 39.
[86] V. S. Thoi, Y. Sun, J. R. Long, C. J. Chang, *Chem. Soc. Rev.* **2013**, *42*, 2388.
[87] J. Timoshenko, B. R Cuenya, *Chem. Rev.* **2021**, *121*, 882.
[88] S. Mondal, D. Bagchi, M. Riyaz, S. Sarkar, A. K. Singh, C. P. Vinod, S. C. Peter, *J. Am. Chem. Soc.* **2022**, *144*, 11859.
[89] Y. Yang, W. H. Lie, R. R. Unocic, J. A. Yuwono, M. Klingenhof, T. Merzdorf, P. W. Buchheister, M. Kroschel, A. Walker, L. C. Gallington, L. Thomsen, P. V. Kumar, P. Strasser, J. A. Scott, N. M. Bedford, *Adv. Mater.* **2023**, *35*, 2305573.
[90] R. Lin, L. Kang, T. Zhao, J. Feng, V. Celorrio, G. Zhang, G. Cibin, A. Kucernak, D. J. L. Brett, F. Corà, I. P. Parkin, G. He, *Energy Environ. Sci.* **2022**, *15*, 2386.
[91] W. Chen, L. Xu, X. Zhu, Y.-C. Huang, W. Zhou, D. Wang, Y. Zhou, S. Du, Q. Li, C. Xie, L. Tao, C.-L. Dong, J. Liu, Y. Wang, R. Chen, H. Su, C. Chen, Y. Zou, Y. Li, Q. Liu, S. Wang, *Angew. Chem., Int. Ed.* **2021**, *60*, 7297.
[92] Z. Yang, B. Zhang, C. Yan, Z. Xue, T. Mu, *Appl. Catal., B* **2023**, *330*, 122590.
[93] S. Li, R. Ma, J. Hu, Z. Li, L. Liu, X. Wang, Y. Lu, G. E. Sterbinsky, S. Liu, L. Zheng, J. Liu, D. Liu, J. Wang, *Nat. Commun.* **2022**, *13*, 2916.
[94] Y. Qi, Y. Zhang, L. Yang, Y. Zhao, Y. Zhu, H. Jiang, C. Li, *Nat. Commun.* **2022**, *13*, 4602.
[95] M. W. Louie, A. T. Bell, *J. Am. Chem. Soc.* **2013**, *135*, 12329.
[96] N. Zhang, X. Feng, D. Rao, X. Deng, L. Cai, B. Qiu, R. Long, Y. Xiong, Y. Lu, Y. Chai, *Nat. Commun.* **2020**, *11*, 4066.
[97] O. Diaz-Morales, D. Ferrus-Suspedra, M. T. M. Koper, *Chem. Sci.* **2016**, *7*, 2639.
[98] K. M. Cole, D. W. Kirk, S. J. Thorpe, *J. Electrochem. Soc.* **2018**, *165*, J3122.
[99] W. Chen, C. Xie, Y. Wang, Y. Zou, C.-L. Dong, Y.-C. Huang, Z. Xiao, Z. Wei, S. Du, C. Chen, B. Zhou, J. Ma, S. Wang, *Chem* **2020**, *6*, 2974.
[100] Z. Liang, D. Jiang, X. Wang, M. Shakouri, T. Zhang, Z. Li, P. Tang, J. Llorca, L. Liu, Y. Yuan, M. Heggen, R. E. Dunin-Borkowski, J. R. Morante, A. Cabot, J. Arbiol, *Adv. Funct. Mater.* **2021**, *31*, 2106349.
[101] T. Wu, X. Zhu, G. Wang, Y. Zhang, H. Zhang, H. Zhao, *Nano Res.* **2018**, *11*, 1004.
[102] L. Wei, M. D. Hossain, M. J. Boyd, J. Aviles-Acosta, M. E. Kreider, A. C. Nielander, M. B. Stevens, T. F. Jaramillo, M. Bajdich, C. Hahn, *ACS Catal.* **2023**, *13*, 4272.
[103] S. Ghosh, B. Dasgupta, S. Kalra, M. L. P. Ashton, R. Yang, C. J. Kueppers, S. Gok, E. G. Alonso, J. Schmidt, K. Laun, I. Zebger, C. Walter, M. Driess, P. W. Menezes, *Small* **2023**, *19*, 2206679.
[104] Z. Li, X. Li, H. Zhou, Y. Xu, S.-M. Xu, Y. Ren, Y. Yan, J. Yang, K. Ji, L. Li, M. Xu, M. Shao, X. Kong, X. Sun, H. Duan, *Nat. Commun.* **2022**, *13*, 5009.
[105] M. Xiang, Z. Xu, Q. Wu, Y. Wang, Z. Yan, *J. Power Sources* **2022**, *535*, 231461.

[106] S. Zhou, Y. Zhao, R. Shi, Y. Wang, A. Ashok, F. Héraly, T. Zhang, J. Yuan, *Adv. Mater.* **2022**, *34*, 2204388.
[107] C. Tang, R. Zhang, W. Lu, Z. Wang, D. Liu, S. Hao, G. Du, A. M. Asiri, X. Sun, *Angew. Chem., Int. Ed.* **2017**, *56*, 842.
[108] B. J. Taitt, D.-H. Nam, K.-S. Choi, *ACS Catal.* **2019**, *9*, 660.
[109] S. Barwe, J. Weidner, S. Cychy, D. M. Morales, S. Dieckhöfer, D. Hiltrop, J. Masa, M. Muhler, W. Schuhmann, *Angew. Chem., Int. Ed.* **2018**, *57*, 11460.
[110] N. Zhang, Y. Zou, L. Tao, W. Chen, L. Zhou, Z. Liu, B. Zhou, G. Huang, H. Lin, S. Wang, *Angew. Chem., Int. Ed.* **2019**, *58*, 15895.
[111] X. Song, X. Liu, H. Wang, Y. Guo, Y. Wang, *Ind. Eng. Chem. Res.* **2020**, *59*, 17348.
[112] B. You, N. Jiang, X. Liu, Y. Sun, *Angew. Chem., Int. Ed.* **2016**, *55*, 9913.
[113] B. You, X. Liu, N. Jiang, Y. Sun, *J. Am. Chem. Soc.* **2016**, *138*, 13639.
[114] G. Sanghez de Luna, T. Tabanelli, J. J. Velasco-Vélez, E. Monti, F. Ospitali, S. Albonetti, F. Cavani, G. Fornasari, P. Benito, *Sustainable Energy Fuels* **2023**, *7*, 4474.
[115] W.-J. Liu, Z. Xu, D. Zhao, X.-Q. Pan, H.-C. Li, X. Hu, Z.-Y. Fan, W.-K. Wang, G.-H. Zhao, S. Jin, G. W. Huber, H.-Q. Yu, *Nat. Commun.* **2020**, *11*, 265.
[116] Y. Li, X. Wei, L. Chen, J. Shi, M. He, *Nat. Commun.* **2019**, *10*, 5335.
[117] R. R. Rao, S. Corby, A. Bucci, M. García-Tecedor, C. A. Mesa, J. Rossmeisl, S. Giménez, J. Lloret-Fillol, I. E. L. Stephens, J. R. Durrant, *J. Am. Chem. Soc.* **2022**, *144*, 7622.
[118] I. Landa-Medrano, M. Olivares-Marín, R. Pinedo, I. Ruiz de Larramendi, T. Rojo, D. Tonti, *Electrochem. Commun.* **2015**, *59*, 24.
[119] T. Takashima, A. Yamaguchi, K. Hashimoto, H. Irie, R. J. E. Nakamura, *Electrochemistry* **2014**, *82*, 325.
[120] Q. Wu, M. Xiao, W. Wang, C. Cui, *ACS Catal.* **2019**, *9*, 11734.
[121] Y. Yan, R. Wang, Q. Zheng, J. Zhong, W. Hao, S. Yan, Z. Zou, *Nat. Commun.* **2023**, *14*, 7987.
[122] P. C. M. Laan, F. J. de Zwart, E. M. Wilson, A. Troglia, O. C. M. Lugier, N. J. Geels, R. Bliem, J. N. H. Reek, B. de Bruin, G. Rothenberg, N. Yan, *ACS Catal.* **2023**, *13*, 8467.
[123] R. M. Van Effen, D. H. Evans, *J. Electroanal. Chem. Interfacial Electrochem.* **1979**, *103*, 383.
[124] M. Yang, Y. Li, C.-L. Dong, S. Li, L. Xu, W. Chen, J. Wu, Y. Lu, Y. Pan, Y. Wu, Y. Luo, Y.-C. Huang, S. Wang, Y. Zou, *Adv. Mater.* **2023**, *35*, 2304203.
[125] T. Wang, L. Tao, X. Zhu, C. Chen, W. Chen, S. Du, Y. Zhou, B. Zhou, D. Wang, C. Xie, P. Long, W. Li, Y. Wang, R. Chen, Y. Zou, X.-Z. Fu, Y. Li, X. Duan, S. Wang, *Nat. Catal.* **2022**, *5*, 66.
[126] D. Yan, C. Mebrahtu, S. Wang, R. Palkovits, *Angew. Chem., Int. Ed.* **2023**, *62*, 202214333.
[127] G. Li, G. Han, L. Wang, X. Cui, N. K. Moehring, P. R. Kidambi, D.-e. Jiang, Y. Sun, *Nat. Commun.* **2023**, *14*, 525.
[128] Q. Qian, J. Zhang, J. Li, Y. Li, X. Jin, Y. Zhu, Y. Liu, Z. Li, A. El-Harairy, C. Xiao, G. Zhang, Y. Xie, *Angew. Chem., Int. Ed.* **2021**, *60*, 5984.
[129] X. Cui, M. Chen, R. Xiong, J. Sun, X. Liu, B. Geng, *J. Mater. Chem. A* **2019**, *7*, 16501.
[130] R. Luo, Y. Li, L. Xing, N. Wang, R. Zhong, Z. Qian, C. Du, G. Yin, Y. Wang, L. Du, *Appl. Catal., B* **2022**, *311*, 121357.
[131] T. Kahlstorf, J. Niklas Hausmann, I. Mondal, K. Laun, I. Zebger, T. Sontheimer, P. W. Menezes, *Green Chem.* **2023**, *25*, 8679.
[132] Q. Xue, Z. Xia, W. Gou, J. Bu, J. Li, H. Xiao, Y. Qu, *ACS Catal.* **2023**, *13*, 400.
[133] A. Kowal, S. N. Port, R. J. Nichols, *Catal. Today* **1997**, *38*, 483.
[134] G. K. Schweitzer, L. L. Pesterfield, *The Aqueous Chemistry of the Elements*, Oxford University Press, Oxford **2010**.
[135] Y. Shi, W. Du, W. Zhou, C. Wang, S. Lu, S. Lu, B. Zhang, *Angew. Chem., Int. Ed.* **2020**, *59*, 22470.
[136] X. Gao, X. Bai, P. Wang, Y. Jiao, K. Davey, Y. Zheng, S.-Z. Qiao, *Nat. Commun.* **2023**, *14*, 5842.
[137] C. Chen, H. Wen, P.-P. Tang, P. Wang, *ACS Sustainable Chem. Eng.* **2021**, *9*, 4564.
[138] L. Trotochaud, S. L. Young, J. K. Ranney, S. W. Boettcher, *J. Am. Chem. Soc.* **2014**, *136*, 6744.
[139] W. Wang, Y. Wang, R. Yang, Q. Wen, Y. Liu, Z. Jiang, H. Li, T. Zhai, *Angew. Chem., Int. Ed.* **2020**, *59*, 16974.
[140] P. Aggarwal, D. Sarkar, K. Awasthi, P. W. Menezes, *Coord. Chem. Rev.* **2022**, *452*, 214289.
[141] Y. Lu, J. Wang, L. Yu, L. Kovarik, X. Zhang, A. S. Hoffman, A. Gallo, S. R. Bare, D. Sokaras, T. Kroll, V. Dagle, H. Xin, A. M. Karim, *Nat. Catal.* **2019**, *2*, 149.
[142] C. Ling, X. Niu, Q. Li, A. Du, J. Wang, *J. Am. Chem. Soc.* **2018**, *140*, 14161.
[143] Y. Huang, X. Chong, C. Liu, Y. Liang, B. Zhang, *Angew. Chem., Int. Ed.* **2018**, *57*, 13163.
[144] J. N. Hausmann, P. W. Menezes, *Appl. Catal., B* **2024**, *342*, 123447.
[145] S. Ghosh, J. N. Hausmann, L. Reith, G. Vijaykumar, J. Schmidt, K. Laun, S. Berendts, I. Zebger, M. Driess, P. W. Menezes, *Adv. Energy Mater.* **2024**, https://doi.org/10.1002/aenm.202400356.
[146] P. Salunkhe, M. Ali A V, D. Kekuda, *Mater. Res. Express* **2020**, *7*, 016427.
[147] G. Gonella, E. H. G. Backus, Y. Nagata, D. J. Bonthuis, P. Loche, A. Schlaich, R. R. Netz, A. Kühnle, I. T. McCrum, M. T. M. Koper, M. Wolf, B. Winter, G. Meijer, R. K. Campen, M. Bonn, *Nat. Rev. Chem.* **2021**, *5*, 466.
[148] A. Erbe, M. F. Tesch, O. Rüdiger, B. Kaiser, S. DeBeer, M. Rabe, *Phys. Chem. Chem. Phys.* **2023**, *25*, 26958.

Suptish Ghosh is currently pursuing his Ph.D. at the Department of Metalorganics and Inorganic Materials, Technical University of Berlin in Germany, under the supervision of Dr. P. W. Menezes and Prof. Dr. Matthias Driess. Prior to this, he obtained his integrated BS-MS degree from the Indian Institute of Science Education and Research, Kolkata (IISER-K), where he worked on electrocatalyst design and their applications, under the supervision of Prof. V. Mahalingam. His ongoing Ph.D. work focuses on developing nickel-based catalysts for water and organic oxidation reactions under industrially relevant conditions, emphasizing the understanding of their reconstruction behavior and catalytic efficacy.

Debabrata Bagchi is currently working as a postdoctoral researcher under the guidance of Dr. P. W. Menezes in Materials Chemistry Group for Thin Film Catalysis, CatLab, Helmholtz-Zentrum Berlin für Materialien und Energie, Germany. He received his Ph.D. degree in Chemical Science from JNCASR, Bangalore under the supervision of Prof. Sebastian C. Peter, after completing his M.Sc. in Chemistry from IIT Madras. His research endeavors are currently focused on the design of catalyst materials, the exploration of dynamic phenomena, and the investigation of mechanisms for various electrocatalytic reactions such as water splitting, CO_2 reduction, and oxidation of organic compounds.

Indranil Mondal obtained his Ph.D. in 2017 from AcSIR, CSIR-CMERI on photocatalytic water splitting. He was an Alexander von Humboldt postdoctoral research fellow at Technische Universität Berlin, Germany from 2020 to 2023. He is currently a SERB-Ramanujan fellow at the Institute of Science Education and Research, Thiruvananthapuram (IISER-TVM). His research interest includes the synthesis of functional materials for energy conversion applications.

Rajenahally V. Jagadeesh is a Group Leader at Leibniz Institute for Catalysis (LIKAT), Germany. He is also a Visiting Professor at VSB-Technical University of Ostrava, Czech Republic and at REVA University, Bangalore, India. He obtained a Ph.D. (2006) from Bangalore University, India. After having performed Postdoctoral Research (2006–2008) at the University of Florida, USA, and worked as an Assistant Professor (2009–2010) at VIT University, India, he joined LIKAT, Germany in the year 2010. The research work of his group focuses on catalysis for sustainable organic synthesis, as well as the valorization of renewable feedstocks and plastics-waste.

Prashanth W. Menezes is a head of materials chemistry for the thin-film catalysis group at CatLab of the Helmholtz- Zentrum Berlin für Materialien und Energie and inorganic materials group leader at Technische Universität Berlin. He received his Ph.D. from the Max Planck Institute for Chemical Physics of Solids in Dresden, following which he moved to Technische Universität München and then to Technische Universität Berlin to work on catalysis. His research focuses on the design, development, and dynamic understanding of unconventional catalysts in heterogeneous catalysis, especially in the area of redox oxygen catalysis and (photo)electrocatalytic water splitting, and electrochemical redox reactions.